

THEORETICAL STUDY OF THE
EARTHQUAKE RESPONSE OF THE
PARADISE COOLING TOWER

Prepared by

T. Y. Yang, C. S. Gran, and J. L. Bogdanoff
School of Aeronautics and Astronautics
Purdue University
West Lafayette, Indiana

Submitted to

THE NATIONAL SCIENCE FOUNDATION

June 3, 1976

BIBLIOGRAPHIC DATA SHEET	1. Report No. NSF/RA-760715	2.	3. Recipient's Accession No.
4. Title and Subtitle Theoretical Study of the Earthquake Response of the Paradise Cooling Tower		5. Report Date June 3, 1976	
7. Author(s) T. Y. Yang, C. S. Gran, J. L. Bogdanoff		8. Performing Organization Rept. No.	
9. Performing Organization Name and Address Purdue University School of Aeronautics and Astronautics West Lafayette, IN 47906		10. Project/Task/Work Unit No.	
12. Sponsoring Organization Name and Address Research Applied to National Needs (RANN) National Science Foundation Washington, D.C. 20550		11. Contract/Grant No. GI41897	
15. Supplementary Notes		13. Type of Report & Period Covered	
16. Abstracts A detailed dynamic analysis, presented in a series of reports, was conducted on the seismic response and structural safety of key subsystems (steam generator, high pressure steam piping, coal handling equipment, cooling tower, chimney) of Unit #3 of TVA at Paradise, Kentucky in order to: (1) determine for the key components the natural frequencies below 50 Hz and the corresponding normal modes; (2) determine response of plant to seismic disturbances; (3) verify through full scale tests results obtained in (1) and determine estimates of damping needed in (2); (4) determine potential failure modes of major structural components; and (5) determine a spare parts policy for a power system so that outages due to damage from seismic disturbances are minimal. Analytical and experimental methods are used. In this study, the dynamic behavior of the cooling tower is analyzed, using quadrilateral plate and beam elements oriented arbitrarily in space, following analysis and confirmation of their predictive value. Response to 1940 El Centro earthquake parameters is studied, and assumed viscous damping coefficients are considered. Comprehensive results, based on this response, are given.		14.	
17. Key Words and Document Analysis. 17a. Descriptors Earthquakes Earthquake resistant structures Safety Hazard Earth movements Safety engineering Cooling towers 17b. Identifiers/Open-Ended Terms Paradise cooling tower 17c. COSATI Field/Group			
18. Availability Statement NTIS		19. Security Class (This Report) UNCLASSIFIED	21. No. of Pages 81
		20. Security Class (This Page) UNCLASSIFIED	22. Price PC A05 / MF A01

THEORETICAL STUDY OF THE
EARTHQUAKE RESPONSE OF THE
PARADISE COOLING TOWER

T. Y. Yang, C. S. Gran, and J. L. Bogdanoff

Any opinions, findings, conclusions
or recommendations expressed in this
publication are those of the author(s)
and do not necessarily reflect the views
of the National Science Foundation.

Summary Report

Prior to 1974 there has been no detailed dynamic analysis of the seismic structural response and safety of large fossil-fuel steam generating plants. In March, 1974, under NSF Grant GI41897, a detailed dynamical analysis was begun on the seismic response and structural safety of key subsystems

(steam generator,
high pressure steam piping,
coal handling equipment,
cooling tower,
chimney)

of Unit #3 of TVA at Paradise, Kentucky to accomplish the following objectives:

- a) Determine for the key components the natural frequencies below 50 Hz and the corresponding normal modes.
- b) Determine response of plant to seismic disturbances.
- c) Verify through full scale tests, where possible, results obtained in a), and determine estimates of damping needed in b).
- d) Determine potential failure modes of major structural components.
- e) Determine a spare parts policy for a power system so that outage due to damage from seismic disturbances are minimal.

Analytical and experimental methods are used.

The attached Reports present what has been accomplished to date.

Before making a few summarizing remarks on the individual Reports, some comments must be made in order to provide perspective on the study.

Paradise, Unit #3 of TVA was selected for study because near-by mine operations provide excitation (due to blasting) for the plant, and TVA was willing to cooperate in the conduct of the study. It should be pointed out that this plant was not designed to resist earthquakes. However, it was felt that this disadvantage was outweighed by the experimental possibilities.

The key components selected for study are critical for operation of the plant and would cause significant outage if damaged. All components can be studied using similar types of analyses. These are the basic reasons for including in this study only the steam generator, high pressure piping, coal handling equipment, cooling tower, and chimney.

Basic data for the analyses were obtained from drawings provided by TVA and Babcock-Wilcox. In addition to these data, a number of assumptions had to be introduced into the analyses. These assumptions refer in the main to the nature of the connections among elements of known properties, the

fixity of columns, the properties of hanger elements, etc. Choices were made based on physical as well as computational reasons.

The analyses were confined to the linear range. After such a study, it is possible to assess at what level of excitation parts of the structure become nonlinear.

Structure-foundation interaction was neglected. Unit #3 of Paradise rests on excavations in limestone. It is assumed that there is little interaction. However, experimental studies will be made on this point.

It was decided at the start that all computations would be carried out with an existing computer program. SAP IV was chosen. Some program modifications have proved necessary, but these have been relatively minor. To obtain familiarity with the program it was necessary to study a number of special cases of the actual structure to ensure that it was functioning properly. For example, substructures within the steam generator support were considered separately; assumed values of viscous damping coefficients were used in generating time histories*; etc. We found the program execution

* It should be noted that the magnitude of the response with zero damping must be interpreted with some caution as systems with slightly different frequencies can exhibit significantly different magnitudes of response.

time slow in some respects which indicates that some of its internal subroutines, such as eigen value solution, could be improved. It is beyond the scope of this project, however, to improve existing programs.

The experimental part of the study has proved much more difficult to conduct than anticipated. TVA has been most cooperative. However, the sheer physical size of the units, the weather, etc. have caused a number of difficulties that were not easy to foresee. Progress is gradually being achieved.

Interest in simple models stems from their possible use in design studies. It was decided to develop a methodology for constructing simple models. At present, our simple models are in the embryonic stage. It is hoped that after the study of two more plants a useful methodology can be obtained. Simple models developed could have been used for one component under study; however, timing made this impossible.

No recommendations will be made or conclusions drawn at this time, except in special situations. The partial examination of one plant does not provide a sufficient basis for such actions. At the completion of the study conclusions and recommendations will be presented.

A number of factors of some importance have not been considered so far. For example, the steam generator's internal elements can move with respect to it, the steam piping exerts dynamic forces on its supports, dynamic stresses in steam piping are just part of its stress system, many different seismic excitations are available, plus many more. Also a spare parts policy was not considered. As additional progress is made, we shall consider some of these problems. However, it must be recognized that it is possible to consider in this study only those factors of major importance. A spare parts policy involves economic considerations; it may not be possible to acquire the information needed to address this point.

Contact with industry in this country and Japan clearly indicates that the current detailed study is of great interest.

An Advisory Committee consisting of

Carl L. Canon	- Babcock & Wilcox Product Design Supervisor for Structural Steel and Design
William A. English	- Tennessee Valley Authority Head Civil Engineer
Clinton H. Gilkey	- Combustion Engineering, Inc. Manager, Engineering Science
Richard F. Hill	- Federal Power Commission Acting Director, Office of Energy Systems

R. Bruce Linderman - Bechtel Power Corporation
Engineering Specialist
D. P. Money - Foster-Wheeler Corporation
Supervisor of Stress Analysis
R. D. Sands - Burns & McDonnell
Chief Mechanical Engineer
Erwin P. Wollak - Pacific Gas & Electric Company
Supervisor, Civil Engineering
Division

has been formed to provide a forum for an interchange of practical and conceptual views on various aspects of the study. The aim is to ensure that what is developed (in simple models) will be of practical use to industry. The Advisory Committee has met twice and reviewed plans and the progress of the investigation.

Contact is also maintained with the following firms:

Mitsubishi Heavy Industries
Babcock-Hitachi
Ishikawajima Harima Heavy Industries
Kawasaki Heavy Industries
Taiwan Power Company

The initial visit provided considerable information on the methods they have used in seismic response studies conducted by the research groups in each organization and plant experience under seismic disturbances.

Comments from the Advisory Committee and reviewers have been most helpful and encouraging. Many of the comments have been considered. However, it is not possible to take account in our studies of all points that have been brought to our attention.

Five professors, 8-10 graduate students, 2 technicians, and a secretary devoted part time to the study. A great deal of effort was devoted to acquiring information and equipment. The cooperation of TVA and Babcock-Wilcox was most helpful and deeply appreciated. Progress was excellent when it is remembered that education of students is a major function of a University.

This research project was sponsored by NSF through Grant No. GI41897.

The Reports in this series are as follows:

Dynamic Behavior of the Steam Generator and Support Structures of the 1200 MW Fossil Fuel Plant, Unit #3, Paradise, Kentucky, by T.Y. Yang, M.I. Baig, J.L. Bogdanoff.

The High Pressure Steam Pipe, by C.T. Sun, A.S. Ledger, H. Lo.

Coal Handling Equipment, by K.W. Kayser and J.A. Euler.

Theoretical Study of the Earthquake Response of the Paradise Cooling Tower, by T.Y. Yang, C.S. Gran, J.L. Bogdanoff.

Theoretical Study on Earthquake Response of a Reinforced Concrete Chimney, by T.Y. Yang, L.C. Shiau, H. Lo.

A Simple Continuum Model for Dynamic Analysis of Complex Plane Frame Structures, by C.T. Sun, H. Lo, N.C. Cheng, and J. L. Bogdanoff.

A Timoshenko Beam Model for Vibration of Plane Frames, by C.T. Sun, C.C. Chen, J.L. Bogdanoff, and H. Lo.



INTRODUCTION

Natural draught cooling towers are hyperbolic paraboloids of revolution in form and are usually made of reinforced concrete of variable thickness. They are generally stiffened at the top and the bottom by ring beams and supported at the base by closely spaced columns. They are vulnerable to seismic disturbances and wind loads. This was evidenced in the spectacular failure of several towers at Ferrybridge, England due to the high velocity wind disturbance in 1965 (Ref. 1). Because the cooling towers are vital to the operation of a large power plant, their dynamic behavior is of considerable interest.

The studies of the behavior of cooling towers have been extensive. Since the membrane shell theory is simpler than the bending shell theory and the base fixity condition produces predominantly membrane state of stress in cooling towers, most of the earlier work on cooling towers was conducted for the case of static analysis with the assumption of fixed base and with the use of membrane theory [see, for example, Ref. 2]. Bending theory has been used in the analysis of the cooling towers with simply-supported base under the static equivalent wind load condition [Ref. 3]. It was pointed out in Ref. 3 that although the bending stresses are not large, the corresponding hoop stresses near the base are significantly different from those obtained by membrane theory.

Earlier dynamic analyses of cooling towers were also conducted for the case of fixed base by the use of membrane theory [see, for example, Ref. 4]. The bending theory of thin elastic shells was later successfully applied to the free vibration analysis of cooling towers with fixed bases. Among the methods of analysis are numerical integration method [Ref. 5],

finite difference method [Ref. 6], and finite element method with the use of rotational ring-type shell elements [Ref. 7]. In reality, however, the cooling towers are supported by discrete columns. These supports provide a condition of physical restraint that is significantly different than the conventional fixed or simply-supported boundary conditions. The effect of discrete column supports must be taken into account if the behaviors of the cooling towers are to be correctly predicted. Efforts on the inclusion of such effects were made for both static and dynamic cases in, among other references, Refs. 8 and 9, by the use of curved rotational shell finite elements. The discrete columns in both Refs. 8 and 9 were modeled by a rotational shell element for which the stiffness and mass properties are equivalent to those of the discrete columns. The free stress state between column joints were modified by applying a system of self-equilibrated edge loadings to the base of the shell.

If the finite element method is chosen to analyze the cooling towers, the most exact way to model the supporting columns appears to be modeling each column as a discrete element through the use of column finite elements with an exact stiffness formulation. To accomplish this, however, one cannot use the rotational shell finite elements, which allow only nodal circles, to join the columns. The quadrilateral shell finite elements must be used instead. In the free vibration analysis of cooling towers, the model using quadrilateral shell elements provides the frequencies in ascending order despite their circumferential mode number while the model using rotational shell elements provides only the frequencies for certain prescribed circumferential mode. For these reasons, the quadrilateral shell finite elements and the column finite elements were chosen to

model the present cooling towers. The description of the elements is given in a separate section.

In this study, the capability of the quadrilateral shell finite elements in predicting natural frequencies of cooling towers is first evaluated through an example of a fixed-base cooling tower. Results for frequencies compared well with previously reported results [Refs. 5-7]. The capability of the column finite elements in modeling the discrete column supports is then evaluated through free vibration analysis of an example of a cooling tower with column supports. Results for frequencies also compared well with a previous alternative solution [Ref. 9].

The two types of finite elements are finally used to model the cooling tower in the 1200 MW Fossil Fuel Steam Generating Power Plant, Unit #3, Paradise, Kentucky (Tennessee Valley Authority). Time-history dynamic response analysis is performed for this cooling tower when subjected to the south-north acceleration component of the 1940 El Centro earthquake for a period of 30 seconds. The 30 second record is broken down into 1500 time steps in the modal superposition analysis. It is found that only the modes that contain one circumferential wave are responsive to the horizontal earthquake disturbance. The results are presented in the form of time-history plots of deflection at the top of the shell and the top of the columns, bending moments at the top and the base of the columns, shearing force and axial force in the columns. The meridional and circumferential deflection shapes are presented at several instances. The distributions of meridional bending moment and meridional membrane force are given for a critical instance. The effect of viscous damping is also considered for several assumed damping coefficients.

Description of the System

There are three cooling towers in the Paradise steam generating plant. The reinforced concrete cooling tower is in the form of a hyperbolic paraboloidal shell of revolution as shown in Fig. 1. The shell thickness varies from 24 inches at the base to 7 inches at the throat and then to 9 inches at the top. The tower is supported by 40 pairs of reinforced concrete columns of circular cross sections. Each pair has a concrete footing buried in the excavated limestone rock. The top of the tower is stiffened by a reinforced concrete ring of rectangular cross section. The top of the ring provides a walk way.

Due to the axisymmetrical nature of the design, both the circumferential and meridional reinforcements vary only along the meridional direction but remain constant along the circumferential direction. The distribution of the equivalent modulus of elasticity for the circumferential reinforcements along the meridional direction is calculated from the design drawings presented in Fig. 2. The distribution of the equivalent modulus of elasticity for the meridional reinforcements along the meridian is presented in Fig. 3. Panels A, B, and C indicate three slightly different types of arrangements in reinforcements in the lower part of the shell.

Finite Elements

Two types of finite elements are used in the modeling of the cooling tower: A three dimensional beam finite element and an orthotropic quadrilateral flat plate finite element oriented arbitrarily in the three dimensional space. The former is used to model the discrete supporting columns and the ring beam at the top of the shell. The latter is used to model the hyperboloidal shell of revolution.

The three dimensional beam finite element has two nodal points, each of which has six degrees of freedom: three displacement degrees of freedom in the three Cartesian coordinate directions and three rotational degrees of freedom about the three Cartesian coordinate axes, respectively. The stiffness matrix is derived on the basis that the axial displacement varies linearly along the element and the transverse deflection varies cubically along the element. The mass matrix is formulated on the basis of lumped masses.

The three dimensional orthotropic quadrilateral plate element is shown in Fig. 4. This element has five degrees of freedom at each corner nodal point: three displacement degrees of freedom \bar{u} , \bar{v} , and \bar{w} in the Cartesian local coordinate directions \bar{x} , \bar{y} , and \bar{z} , respectively; and two slope degrees of freedom about the \bar{x} and \bar{y} axes, respectively. For reasons of computational efficiency, the quadrilateral element is composed of four triangular elements. The four triangles share a common central nodal point which is located at the average of the coordinates of the four corner nodal points. The five degrees of freedom at this central nodal point are eliminated at the elemental level prior to assemblage, thus the quadrilateral element effectively has a total of 20 degrees of freedom, five per nodal point.

The membrane stiffness of each sub-triangular element is represented by the constant strain based on linear displacement functions in both \bar{u} and \bar{v} [Ref. 10]. The flexural stiffness of each sub-triangular element is represented by the fully compatible HCT element based on the cubic displacement functions in \bar{w} [Ref. 11]. The orthotropic material property is included in the formulations for both the membrane and flexural stiffness matrices. The mass matrix of the quadrilateral element is formulated

on the basis of lumped masses. The formulation, with reference to the local coordinates \bar{x} , \bar{y} , and \bar{z} , is given in the following symbolic form

$$\{\bar{F}\} = [\bar{k}] \{\bar{q}\} + [\bar{m}] \{\ddot{\bar{q}}\} \quad (1)$$

$20 \times 1 \quad 20 \times 20 \quad 20 \times 1 \quad 20 \times 20 \quad 20 \times 1$

where $\{\bar{F}\}$ and $\{\bar{q}\}$ are vectors of nodal forces and displacements, respectively; $[k]$ and $[m]$ are the element stiffness and mass matrices, respectively; the "dot" represents time derivative; and the "bar" represents local coordinates.

Through a congruent coordinate transformation technique, the element formulation (1) in local coordinates is transformed into the formulation in global coordinates,

$$\{F\} = [T]^T [k] [T] \{q\} + [T]^T [m] [T] \{\ddot{q}\} \quad (2)$$

$24 \times 1 \quad 24 \times 20 \quad 20 \times 20 \quad 20 \times 24 \quad 24 \times 1 \quad 24 \times 20 \quad 20 \times 20 \quad 20 \times 24 \quad 24 \times 1$

where the matrix $[T]$ is the coordinate transformation matrix. This coordinate transformation generates six degrees of freedom at each nodal point: three displacement degrees of freedom u , v , and w in the global coordinate directions, x , y , and z , respectively; and three rotational degrees of freedom θ_x , θ_y , and θ_z about the x , y , and z axes, respectively. Formulation (2) for each individual element can thus be used in the three dimensional space to model shell structures.

When compared with the popular ring-type rotational shell finite element, the quadrilateral elements appear to have two advantages. First, the quadrilateral elements provide nodal points that can join the column elements while the ring elements can only provide nodal circles. Second,

the quadrilateral elements provide the natural frequencies in ascending order while the ring elements only give the natural frequencies for each specified circumferential mode.

Assumptions

The following assumptions underlie this study:

- (1) Since the column footings are imbedded in limestone rock, the bases of the supporting columns are assumed to be fixed.
- (2) The reinforced concrete cooling tower behaves elastically.
- (3) The shell material is orthotropic. Moduli of elasticity are different in the circumferential and longitudinal directions.

Results

In order to substantiate the reliability of the results obtained through the use of the present beam and quadrilateral plate elements, it is necessary to compare their performance with that of alternative methods. This is accomplished by means of two examples for which frequencies have been previously determined using various techniques. The first example is one in which the base of the hyperboloidal shell is fixed; the second has "discrete" supporting columns.

(1) Free Vibration Analysis of an Example of Cooling Tower with Fixed Base.

The first example is described in Fig. 5. The isotropic modulus of elasticity of the reinforced concrete cooling tower is 3×10^6 psi; the Poisson's ratio is 0.15; and the mass density is 0.225×10^{-3} lbs-sec²/in⁴. The base of the tower is assumed to be rigidly fixed. This example was analyzed previously by Carter, et al. [Ref. 5] using numerical integration technique; by Hashish and Abu-Sitta [Ref. 6] using finite difference

technique; and by Sen and Gould [Ref. 7] using curved rotational shell finite elements. Their results for the natural frequencies are shown in Table 1.

In this study, three different finite element meshes are used: 4x16, 6x20, and 8x20, respectively. The three meshes correspond to 384, 720, and 960 degrees of freedom, respectively. The present results are shown in Table 1 for comparison. It is seen that for the 4x16 mesh, the frequencies are, in general, higher than those from the alternative solutions [Refs. 5-7]. These discrepancies are, however, within tolerable range from a practical engineering point of view. For the 6x20 mesh, the frequencies, in general, reduce slightly. For the 8x20 mesh, the frequencies reduce further and are in close agreement with those from the previous solutions [Refs. 5-7]. It may reasonably be concluded from this example that the quadrilateral elements are adequate for the dynamic analysis of cooling towers with fixed base. The CDC 6500 central processing times for computing all the frequencies by each mesh are given in Table 1. The time for calculating the modes with one circumferential wave is, however, not included. It is noted that in obtaining the frequencies shown in Table 1 by Sen and Gould [Ref. 7], 6 to 13 rotational shell finite elements were used for each assumed number of circumferential waves.

(2) Free Vibration Analysis of an Example of Cooling Tower with Discrete Supporting Columns.

An example of reinforced concrete cooling tower with discrete supporting columns has been treated by Gould et al. [Ref. 9] by the use of curved rotational shell finite elements. The supporting columns were modeled by a special rotational elastic element whose stiffness and mass properties are equivalent to those of the discrete columns. This element

has the same degrees of freedom at the nodal circles as those assumed in the shell element.

The example is described in Fig. 6. The cooling tower has 88 supporting columns with cross sectional area of 52 by 24 square inches. For the concrete in both the shell and the columns, the modulus of elasticity, the Poisson's ratio, and the mass density were assumed to be 4×10^6 psi, $1/6$, and 0.225×10^{-3} lbs-sec²/in⁴, respectively.

In Ref. 9, the cooling tower was first analyzed with the base fixed and then with the base supported by the 88 discrete columns. Part of the results for natural frequencies are shown in Table 2.

For the case of fixed base, the present results obtained by the use of 8x20 mesh (960 degrees of freedom) agree reasonably well with those obtained by Gould et al. by 14 rotational shell finite elements (see Table 2). For the case with discrete supporting columns, the present results obtained by the use of 8x22 mesh (1320 degrees of freedom) are, in general, lower than those obtained by Gould et al. (See Table 2). This may imply that the present realistic column modeling provides a less stiff representation than the equivalent rotational shell element. It should be noted that the time used in computing the modes with one circumferential wave is not included in Table 3.

As shown in Fig. 7 for the modeling with 8x22 mesh, the lowest row is modeled by 66 triangular elements instead of 22 quadrilateral elements. Each supposedly quadrilateral element is divided into three triangular elements with two nodes on the top and three nodes at the bottom. By doing so, 44 nodes are created which can be connected to the top joints of the 44 pairs of column finite elements.

With the successful completion of the first two examples, it is reasonably convincing that the combined usage of quadrilateral shell elements and beam elements will quite accurately predict the dynamic behavior of the column supported cooling towers. The cooling tower in the Paradise Steam Generating Plant is then analyzed in this manner.

(3) Free Vibration Analysis of the Paradise Cooling Tower.

In the free vibration analysis of the Paradise cooling tower, three different quadrilateral shell element modelings are used: 4x16 mesh; 6x20 mesh; and 8x20 mesh, respectively. The first modeling has 16 beam finite elements at the top of the shell to represent the stiffened ring beam. The other two modelings use 20 stiffened beam elements for this purpose. In the three modelings, each quadrilateral element in the base row is divided into three triangular elements (see Fig. 7) so that it has three nodal points at the base line. Thus for the 6x20 and 8x20 meshes, the base circle of the tower has 40 nodes that can be connected to the 40 pairs of discrete column elements. For the 4x16 mesh, the 40 pairs of columns are replaced by 32 pairs of equivalent columns. The three modelings thus have 576, 960, and 1200 degrees of freedom, respectively.

Since the arrangement of the reinforcements in the circumferential direction is different than that in the meridional direction, each quadrilateral shell finite element must be orthotropic. The distributions of the equivalent moduli of elasticity in the circumferential and meridional directions are shown in Figs. 2 and 3, respectively. The input of moduli of elasticity for the orthotropic quadrilateral shell element is based on such distributions.

The present results for the natural frequencies of several modes using different meshes are given in Table 3. The first two meridional mode shapes for the third through seventh circumferential modes are shown in Figs. 8 and 8a. It is seen that the base of the shell moves considerably due to the flexible nature of the column supports. This phenomenon cannot be predicted if the base of the shell is assumed as fixed. Figures 8 and 8a also show the meridional mode shapes for the hypothetical case that the base of the shell is fixed. It is interesting to see the manner in which the flexible column supports affect the meridional mode shapes.

It is important to point out that when the circumferential mode number is equal to one, the shell vibrates in a side-swaying type of motion. When the circumferential mode number is not equal to one, the shell vibrates in a breathing type of motion. Previous studies [Refs. 4 and 9] have pointed out that only the modes with one circumferential wave are excitable by the horizontal earthquake motion.

(4) Free Vibration Modes of Cooling Towers with One Circumferential Wave.

The modes with one circumferential wave are usually not within the frequency range of lower modes. For the example of a cooling tower with fixed base (see Fig. 5), the first three side-swaying mode frequencies are shown in Table 1 as 3.119, 7.1638, and 11.317 Hz., respectively. These values are considerably higher than the other breathing mode frequencies shown in the table. For the purpose of saving computing time, the inertial terms associated with the horizontal direction perpendicular to the earthquake direction are neglected from the mass matrices so that some of the breathing modes may be skipped and the side-swaying modes may arrive early. By doing so, the present three side-swaying modes come as the 20th, 37th, and 46th modes, respectively. Because the search of modes

with one circumferential wave is expensive, it is done in this study by a relatively coarse mesh (4x16). It is, however, seen in Table 1 that the three frequencies obtained by the 4x16 mesh are very close to the previous three alternate solutions. The meridional mode shapes for the three modes are shown in Fig. 9. The circumferential mode shapes remain circular for all three modes.

For the Paradise cooling tower, the first two natural frequencies for the modes with one circumferential wave obtained by the 4x16 mesh are given in Table 3. The two frequency values are 2.19 and 4.26 Hz, respectively. During the computation, they come as the 8th and 34th modes, respectively. The corresponding meridional mode shapes are shown in Fig. 10. The circumferential mode shapes remain circular.

After the modes with one circumferential wave are found, the dynamic response to the horizontal earthquake can be determined.

(5) Earthquake Response of the Example Cooling Tower with Fixed Base.

The time-history response of the example cooling tower with fixed base (Fig. 5) subjected to a horizontal component of the El Centro earthquake is first analyzed. The south-north component of acceleration for 30 seconds is shown in Fig. 11. Because this component diminishes considerably after 30 seconds, only 30 seconds are considered in this time-history analysis. The method of modal superposition is used. The 30 second record is broken down into 1500 time steps with a time interval of 0.02 seconds. In the output for the time-history plots, the time interval is 0.08 seconds.

Two separate analyses are carried out for this example. The first

analysis includes the first side-swaying mode and all the lower breathing modes. The second analysis includes the first two side-swaying modes and all the lower breathing modes. The second set of results are, in general, quite close to the first set of results. For illustrative purpose, only the first set of results are presented.

The time-history response for the tip deflection at $\theta=0^\circ$ (the circumferential angle measured from the direction of the earthquake) is shown in Fig. 12. The maximum deflection is -1.49 inches at 4.48 seconds. The deflection begins to decrease after 14 seconds. The deflection shapes along the meridional line at $\theta=0^\circ$ at three critical instances are shown in Fig. 13. The circumferential deflection shapes at the top of the shell at three critical instances are shown in Fig. 14. The shapes are no longer circular. The circumferential deflection shapes at the throat (270 feet above ground) are shown in Fig. 15 for four instances. They remain very close to circular shapes.

(5) Earthquake Response of the Paradise Cooling Tower with Discrete Supporting Columns.

Again, the south-north component of the May 1940 El Centro earthquake, as described in the previous section, is considered in determining the response of the Paradise Plant cooling tower with discrete supporting columns. The 4x16 mesh with 576 degrees of freedom is used. The analysis includes all modes up to the first side-swaying mode.

The time-history response for the deflection at the top of the shell at $\theta=0^\circ$, where θ is defined as the circumferential angle measured from the direction of the earthquake, is shown in Fig. 16. The maximum deflection is found to be 7.36 inches, arriving at 9.20 seconds.

The response for the deflection at the top of the column at $\theta=0^\circ$ is shown in Fig. 17. The maximum deflection is -0.861 inches at 11.04 seconds. These deflections are considerably smaller than those at the top of the shell. They should not, however, be neglected as in the assumed case with fixed base.

The longitudinal deflection shapes along a meridional line at $\theta=0^\circ$ are shown in Fig. 18 for three critical instances. The corresponding circumferential mode shapes at the top, at nearly half way (240 feet above ground), and at the base (top of the columns) of the shell are shown in Figs. 19, 20, and 21, respectively. It is seen that the circumferential deflection shapes remain very close to circular shape at both the top and the base of the shell. They are no longer of circular shape at nearly half way of the shell.

The time-history responses of the bending moment at the column base at $\theta=5.6^\circ$ and at the column top at $\theta=0^\circ$ are shown in Figs. 22 and 23, respectively. The bending moment is defined as the one about the line which is tangential to the base circumference and perpendicular to the axis of the column. The magnitudes of bending moment at the top of the columns are substantially larger than those at the base of the column. The maximum bending moments are 408.5 ft-kips at the top and 122.8 ft-kips at the base, both occurred at 9.2. seconds. The bending moment at the top produces 22.5 Ksi maximum tensile stress in the outmost reinforced bar and 3168 psi maximum compressive stress in the concrete.

The time-history response of the shearing force in the column (constant through the column) at $\theta=0^\circ$ is shown in Fig. 24. The shearing force is acting in the same direction as the earthquake. The maximum shearing force is 12,180 pounds at 9.2 seconds. This magnitude is quite

small since it produces a shearing stress of only 22.43 psi in the concrete column. It is noted that a check on the free body of the column shows that, at 9.2 seconds, the shearing force and the two bending moments at the ends satisfy equilibrium.

The time-history response of the axial force in the column at $\theta=0^\circ$ is shown in Fig. 25. The maximum axial force is 3282 kips in compression at 9.2 seconds. This axial force produces a stress of 4447 psi in concrete. It also produces 31.6 ksi in reinforced bar if the concrete is assumed as ineffective in carrying load.

It is important to note that in the presentation of Figs. 22-25 and in computing all the column stresses, the columns are referred to as the equivalent columns rather than the original column. As described previously, the 4x16 mesh only allows the connections to 32 pairs of equivalent columns instead of the 40 pairs of original columns. In the following presentations, the columns are also referred to as equivalent columns.

The distribution of meridional bending moment at $\theta=0^\circ$ and at the most critical time of 9.2 seconds is shown in Fig. 26. This moment is acting about the circumferential tangent line at $\theta=0^\circ$. It is interesting to see that approximately 100 feet above the ground, the moment becomes nearly zero which shows the predominant membrane behavior. The maximum bending moment is 26,570 ft-lbs/ft which produces a maximum meridional bending compressive stress of 2219 psi in concrete and a maximum tensile stress of 5325 psi in the reinforcing bar. It should be noted that, due to the coarse mesh used, the present results for stresses include some degree of error.

The distribution of meridional membrane force at $\theta=0^\circ$ and at 9.2

seconds is shown in Fig. 27. It is seen that this force steadily increases from zero at the top to its maximum at the base of the shell. The maximum membrane force is 210 kip/ft which produces a stress of 1730 psi in concrete if it is in compression and 12.3 ksi in the reinforcing bar if it is in tension.

Since the circumferential deflection shapes are, in general, close to circles at almost all levels of the shell, the results for circumferential bending moment and circumferential membrane forces are found to be quite small in this problem. Therefore, these results are not shown.

(7) Effect of Viscous Damping.

Since the viscous damping coefficients for the Paradise cooling tower are not known, only assumed values are used in this study. It is assumed that all the modes have the same viscous damping coefficient. Three different values of damping coefficient are assumed for this cooling tower: 4 percent; 7 percent; and 10 percent of its critical value.

The time-history responses for the tip deflection, column top deflection, bending moment at column top, and axial force in the column (all at $\theta=0^\circ$ for the Paradise cooling tower with the three different damping coefficients are shown in Figs. 28-39. In Figs. 28-33, the deflection is defined as moving in the direction of earthquake. In Figs. 34-36, the bending moment is defined as acting about the line perpendicular to the column axis and tangent to the circumference of the shell base. It is seen in Figs. 28-39 that all quantities reduce progressively as the value of damping coefficient increases. These sets of results should provide a basis for estimating the effect of damping with a given coefficient values.

As a different way of presentation, the variation of the maximum shell tip deflection ratio (at $\theta=0^\circ$) versus the damping coefficient is plotted in Fig. 40. The maximum tip deflection ratio is defined as the ratio between the maximum tip deflection with damping and the tip deflection at 9.2 seconds with no damping. The variation of the maximum column top deflection ratio versus damping coefficient is also presented in the same figure. The two curves are almost identical. It is seen that the damping coefficient with 4 percent of its critical value reduces the deflection by 60 percent. The effect of increase in damping coefficient beyond 4 percent is less pronounced.

The variation of the maximum bending moment ratio at the top of the column (at $\theta=0^\circ$) versus the damping coefficient is shown in Fig. 41. The ratio is with reference to the bending moment at the top of the column at 9.2 seconds with no damping. The variation of the maximum axial force ratio in the column at $\theta=0^\circ$ versus damping coefficient is shown in Fig. 42. Again, the ratio is with reference to the column axial force at 9.2 seconds with no damping. The trends of the curves in both Figs. 41 and 42 are the same as those observed in Fig. 40.

Concluding Remarks

In this study, the quadrilateral plate elements and the beam elements, both oriented arbitrarily in the three-dimensional space, are used in the analysis of dynamic behaviors of cooling towers. Free vibration analyses for two examples of cooling towers, one with base fixed and one with discrete supporting columns, are first performed with results in satisfactory agreement with previous alternative solutions. The earthquake responses of the cooling tower in the TVA Steam Generating Plant,

Unit #3, Paradise, Kentucky, subjected to the El Centro earthquake are then studied. Assumed values of viscous damping coefficients are considered. A comprehensive set of results is presented which provides some insights into the dynamic behaviors of a cooling tower in response to an horizontal earthquake. Some conclusions are made as follows.

(1) The combined use of quadrilateral shell elements and column elements not only provides a realistic modeling of the column supported cooling towers but also predicts accurate natural frequencies and modes (see comparisons in Tables 1 and 2).

(2) The 4x16 mesh of quadrilateral elements is practically sufficient for the purpose of predicting gross dynamic behaviors of the cooling towers. For detail stress predictions, however, finer meshes are needed.

(3) The modes with one circumferential wave are the excitable modes by the horizontal earthquake motion. For the present cooling tower and earthquake, the first mode appears to be predominant. The same conclusion was made in Ref. 4.

(4) With the neglect of the inertia forces in the horizontal direction perpendicular to the direction of motion, some breathing modes can be skipped and the modes with one circumferential wave can be obtained early.

(5) The inclusion of the column supports reduces the natural frequencies for the cooling tower originally with fixed base. Such conclusion has been made previously (see, for example, Ref. 9).

(6) The tops of the columns deflect substantially during earthquake. Neglecting the columns in the dynamic analysis is inadequate.

(7) The supporting columns show points of inflection during earthquake response. The bending moments at the tops of the columns are more

critical than those at the bases of the columns.

(8) During earthquake response, the axial forces in the supporting columns are critical.

(9) The membrane behavior dominates in the shell portions sufficiently far from the base.

(10) For the present cooling tower, the inclusion of viscous damping with 4 percent of its critical value reduces the maximum displacements or stresses by about 60 percent. The increase in damping beyond 4 percent, however, has less effect.

REFERENCES

- [1] General Electricity Generating Board, "Report of the Committee of Inquiry into Collapse of Cooling Towers at Ferrybridge," November 1, 1965, Her Majesty's Stationary Office, London.
- [2] Martin, D. W. and Scriven, W. E., "The Calculation of Membrane Stresses in Hyperbolic Cooling Towers," Proceedings, Institute of Civil Engineers, Vol. 19, 1961, pp. 503-513.
- [3] Gould, P. L. and Lee, S. L., "Bending of Hyperbolic Cooling Towers," Journal of the Structural Division, Proceedings of ASCE, Vol. 93, No. ST5, Oct. 1967, pp. 125-146.
- [4] Abu-Sitta, S. H. and Davenport, A. G., "Earthquake Design of Cooling Towers," Journal of the Structural Division, Proceedings of ASCE, Vol. 96, No. ST9, Sept. 1970, pp. 1889-1902.
- [5] Carter, R. L., Robinson, A. R., and Schnobrick, W. C., "Free Vibration of Hyperboloidal Shells of Revolution," Journal of the Engineering Mechanics Division, Proceedings of ASCE, Vol. 95, No. EM5, Oct. 1969, pp. 1033-1052.
- [6] Hashish, M. G. and Abu-Sitta, S. H., "Free Vibration of Hyperbolic Cooling Towers," Journal of the Engineering Mechanics Division, Proceedings of ASCE, Vol. 97, No. EM2, April 1971, pp. 253-269.
- [7] Sen, S. K. and Gould, P. L., "Free Vibration of Shells of Revolution," Journal of the Engineering Mechanics Division, Proceedings of ASCE, Vol. 100, No. EM2, April 1974, pp. 283-303.
- [8] Sen, S. K. and Gould, P. L., "Hyperboloidal Shells on Discrete Supports," Journal of the Structural Division, Proceedings of ASCE, Vol. 99, No. ST3, March 1973, pp. 595-603.
- [9] Gould, P. L., Sen, S. K., and Suryoutomo, H., "Dynamic Analysis of Column Supported Hyperboloidal Shells," Earthquake Engineering and Structural Dynamics, Vol. 2, 1974, pp. 269-279.
- [10] Turner, M. J., et al., "Stiffness and Deflection Analysis of Complex Structures," Journal of Aeronautical Sciences, Vol. 23, No. 9, Sept. 1956, pp. 805-823.
- [11] Clough, R. W. and Tocher, J. L., "Finite Element Stiffness Matrices for the Analysis of Plate Bending," Proceedings of the Conference on Matrix Methods in Structural Mechanics, Air Force Flight Dynamics Lab. Report TR-66-80., Dayton, Ohio, Oct. 1965.

Table 1. The Natural Frequencies (in Hz.) for a Cooling Tower with Base Fixed.

Circumferential Mode	Longitudinal Mode	Carter et al. (numerical integration)	Hashish and Abu-Sitta (finite difference)	Sen and Gould (curved rotational shell elements)	Quadrilateral finite elements		
					4x16 Mesh	6x20 Mesh	8x20 Mesh
1	1	3.2884	3.3345	3.2910	3.3119		
	2	6.7405	6.8816	6.8176	7.1638		
	3	10.5207	10.5316	10.6666	11.3170		
2	1	1.7654	1.7848	1.7662	1.8681	1.8153	
	2	3.6931	3.7234	3.6960			
	3	6.9562	6.9553	7.0058			
3	1	1.3749	1.3929		1.5356	1.4528	1.3627
	2	1.9904	2.0150		2.0969		
	3	4.3254	4.3353				
4	1	1.1808	1.2003	1.1820	1.3830	1.3248	1.2099
	2	1.4475	1.4597	1.4491	1.6136	1.5648	1.4468
	3	2.7777	2.7762	2.7866	2.8882		
5	1	1.0348	1.0441	1.0354	1.2447	1.1808	1.0556
	2	1.4293	1.4417	1.4345	1.5855	1.5806	
	3	2.0559	2.0555	2.0640	2.3176		
	4				3.4110		
6	1	1.1467	1.1544		1.3120	1.2672	1.1382
	2	1.3231	1.3335		1.5492	1.5461	
	3	2.0141	2.0152		2.1702		
	4				2.9107		
7	1	1.3014	1.3055		1.4460	1.4556	1.3230
	2	1.5133	1.5189		1.6040	1.6220	
	3	1.9217	1.9200		2.1470	2.0705	
	4				2.8062		
8	1				1.5059	1.6418	
	2				1.6636	1.8460	
	3				2.1579	2.0647	
	4				2.8110		
CDC 6500 CP time (minutes)					29.0	67.9	38.0

Table 2. The Natural Frequencies (in Hz) for a Cooling Tower with Discrete Column Supports.

Circumferential Mode	Longitudinal Mode	Fixed Base		Column Base	
		Gould et al.	This Study 8x20 Mesh	Gould et al.	This Study 8x22 Mesh
3	1	1.194	1.1854	1.086	1.0921
	2	1.672		1.314	
4	1	1.104	1.1255	0.945	0.9510
	2	1.302	1.3041	1.204	1.1686
5	1	1.131	1.1467	1.032	1.0245
	2	1.453	1.4634	1.256	1.2195
6	1	1.400	1.4055	1.235	1.1893
	2	1.568		1.455	
CDC 6500 CP Time (minutes)			37.6		54.2

Table 3. The Natural Frequencies in Hz. for the Cooling Tower of Paradise Steam Generating Plant.

Circumferential Mode	Longitudinal Mode	4x16 Mesh	6x20 Mesh	8x20 Mesh
1	1 2 3	2.1947 4.2615		
2	1 2	1.2538 1.9882	1.2391	1.2148
3	1 2	0.8875 1.6263	0.8777 1.5321	0.8857 1.4504
4	1 2	0.9851 1.3965	0.9306 1.3592	0.9057 1.3353
5	1 2	0.8446 2.0430	0.8255	0.8491
6	1 2	1.0235 1.9160	1.0763 1.6691	1.0351
7	1 2 3	1.2708 1.9363 2.1250	1.4156 1.7525	1.2997
8	1 2	1.3795 2.0641	1.6789	
CDC 6500 CP Time (minutes)		35.4	43.5	57.4

FIGURE CAPTIONS

- Fig. 1. The Hyperbolic Paraboloidal Cooling Tower in the TVA Steam Generating Power Plant, Unit #3, Paradise, Kentucky.
- Fig. 2 The Distribution of Equivalent Modulus of Elasticity for the Circumferential Reinforcements Along the Meridional Direction.
- Fig. 3. The distribution of Equivalent Modulus of Elasticity for the Meridional Reinforcements Along the Meridional Direction.
- Fig. 4. A Quadrilateral Plate Finite Element in the Three-Dimensional Space.
- Fig. 5. An Example of a Reinforced Concrete Cooling Tower with Base Fixed.
- Fig. 6. An Example of a Reinforced Concrete Cooling Tower with Discrete Column Supports.
- Fig. 7. The Finite Element Modeling of the Example Cooling Tower with Column Supports.
- Fig. 8. The Longitudinal Mode Shapes for the Paradise Cooling Tower with Discrete Supporting Columns and Top Ring Beam ($j =$ Circumferential Mode Number).
- Fig. 8a. Continuation of Fig. 8.
- Fig. 9. The First Three Longitudinal Mode Shapes (with One Circumferential wave) for the Cooling Tower Example (Fig. 5).
- Fig. 10. The First **Two** Longitudinal Mode Shapes (with One Circumferential Wave) for the Paradise Cooling Tower.
- Fig. 11. The South-North Acceleration Component of the El Centro Earthquake in 1940.
- Fig. 12. Time-History Response of Tip Deflection at $\theta=0^\circ$ for the Example Cooling Tower with Fixed Base.

- Fig. 13. Longitudinal Deflection Shapes at $\theta=0^\circ$ for the Example Cooling Tower with Fixed Base.
- Fig. 14. Circumferential Deflection Shapes at the Top of the Example Cooling Tower with Fixed Base.
- Fig. 15. Circumferential Deflection Shapes at the Throat of the Example Cooling Tower with Fixed Base.
- Fig. 16. Time-History Response of Tip Deflection at $\theta=0^\circ$ for the Paradise Cooling Tower.
- Fig. 17. Time-History Response of Deflection at the Top of the Column at $\theta=0^\circ$ for the Paradise Cooling Tower.
- Fig. 18. Longitudinal Deflection Shapes at $\theta=0^\circ$ for the Paradise Cooling Tower.
- Fig. 19. Circumferential Deflection Shapes at the Top of the Paradise Cooling Tower.
- Fig. 20. Circumferential Deflection Shapes of the Paradise Cooling Tower at 240 Feet Above Ground.
- Fig. 21. Circumferential Deflection Shapes at the Base (Top of the Columns) of the Paradise Cooling Tower.
- Fig. 22. Time-History Response of Bending Moment at Column Base at $\theta=5.6^\circ$ for the Paradise Cooling Tower.
- Fig. 23. Time-History Response of Bending Moment at Column Top at $\theta=0^\circ$ for the Paradise Cooling Tower.
- Fig. 24. Time-History Response of Shearing Force in the Column at $\theta=0^\circ$ for the Paradise Cooling Tower.
- Fig. 25. Time-History Response of Axial Force in the Column at $\theta=0^\circ$ for the Paradise Cooling Tower.

- Fig. 26. Distribution of Meridional Bending Moment at $\theta=0^\circ$ for the Paradise Cooling Tower (at 9.2 Seconds).
- Fig. 27. Distribution of Meridional Membrane Force at $\theta=0^\circ$ for the Paradise Cooling Tower (at 9.2 Seconds).
- Fig. 28. Tip Deflection at $\theta=0^\circ$ vs. Time Curve for the Paradise Cooling Tower with Damping Coefficient Equal to 4 Percent of its Critical Value.
- Fig. 29. Tip Deflection at $\theta=0^\circ$ vs. Time Curve for the Paradise Cooling Tower with Damping Coefficient Equal to 7 Percent of its Critical Value.
- Fig. 30. Tip Deflection at $\theta=0^\circ$ vs. Time Curve for the Paradise Cooling Tower with Damping Coefficient Equal to 10 Percent of its Critical Value.
- Fig. 31. Deflection at Column Top (at $\theta=0^\circ$) vs. Time Curve for the Paradise Cooling Tower with Damping Coefficient Equal to 4 Percent of its Critical Value.
- Fig. 32. Deflection at Column Top (at $\theta=0^\circ$) vs. Time Curve for the Paradise Cooling Tower with Damping Coefficient Equal to 7 Percent of its Critical Value.
- Fig. 33. Deflection at Column Top (at $\theta=0^\circ$) vs. Time Curve for the Paradise Cooling Tower with damping coefficient Equal to 10 Percent of its Critical Value.
- Fig. 34. Bending Moment at Column Top (at $\theta=0^\circ$) vs. Time Curve for the Paradise Cooling Tower with Damping Coefficient Equal to 4 Percent of its Critical Value.
- Fig. 35. Bending Moment at Column Top (at $\theta=0^\circ$) vs. Time Curve for the

Paradise Cooling Tower with Damping Coefficient Equal to 7 Percent of its Critical Value.

Fig. 36. Bending Moment at Column Top (at $\theta=0^\circ$) vs. Time Curve for the Paradise Cooling Tower with Damping Coefficient Equal to 10 Percent of its Critical Value.

Fig. 37. Axial Force in the Column (at $\theta=0^\circ$) vs. Time Curve for the Paradise Cooling Tower with Damping Coefficient Equal to 4 Percent of its Critical Value.

Fig. 38. Axial Force in the Column (at $\theta=0^\circ$) vs. Time Curve for the Paradise Cooling Tower with Damping Coefficient Equal to 7 Percent of its Critical Value.

Fig. 39. Axial Force in the Column (at $\theta=0^\circ$) vs. Time Curve for the Paradise Cooling Tower with Damping Coefficient Equal to 10 Percent of its Critical Value.

Fig. 40. Variations of Maximum Tip Deflection Ratio and Maximum Column Top Deflection Ratio vs. Damping Coefficient.

Fig. 41. Variation of Maximum Bending Moment Ratio at Column Top (at $\theta=0^\circ$) vs. Damping Coefficient.

Fig. 42. Variation of Maximum Axial Force Ratio in Column (at $\theta=0^\circ$) vs. Damping Coefficient.

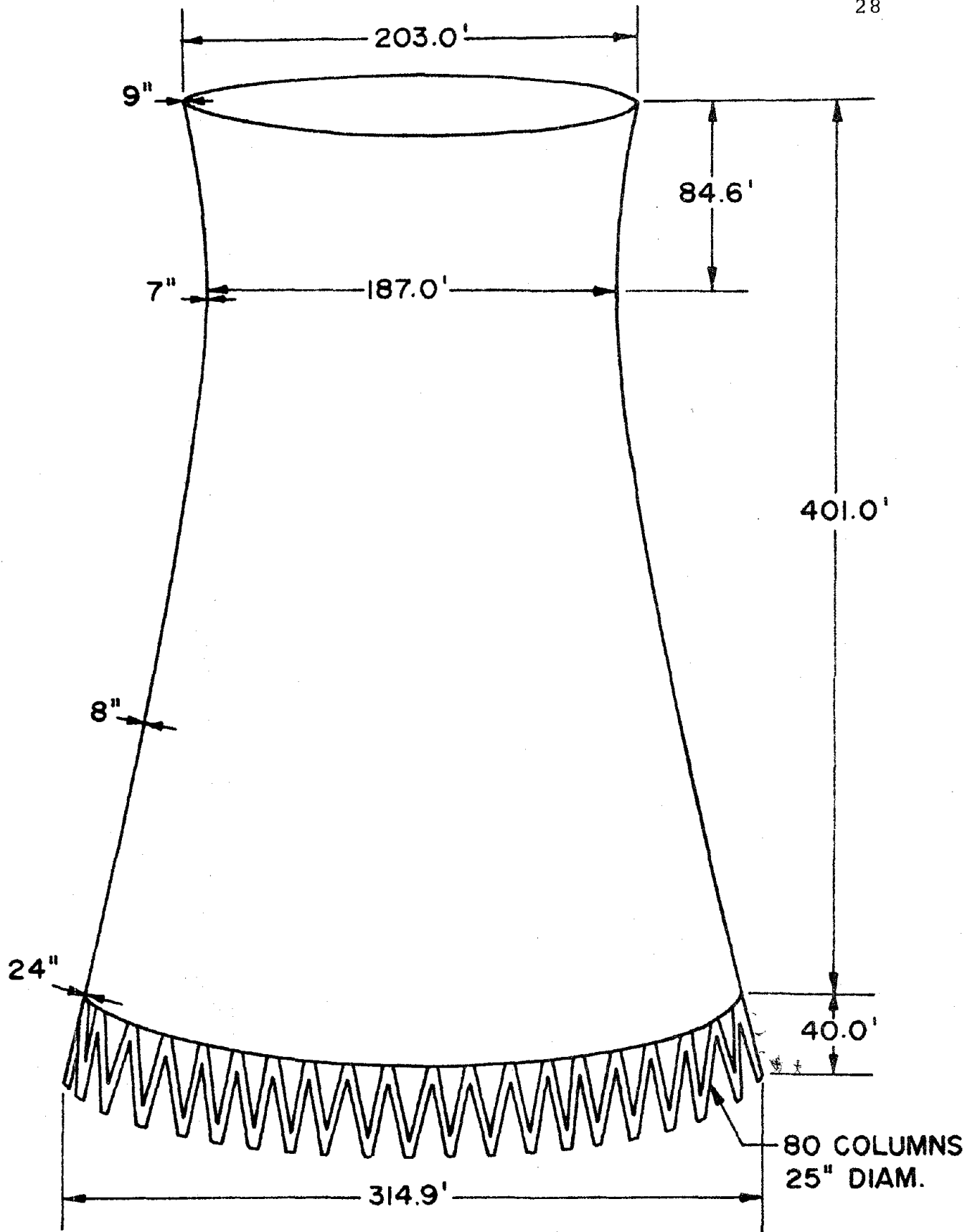


Fig. 1. The Hyperbolic Paraboloidal Cooling Tower in the TVA Steam Generating Power Plant, Unit #3, Paradise, Kentucky.

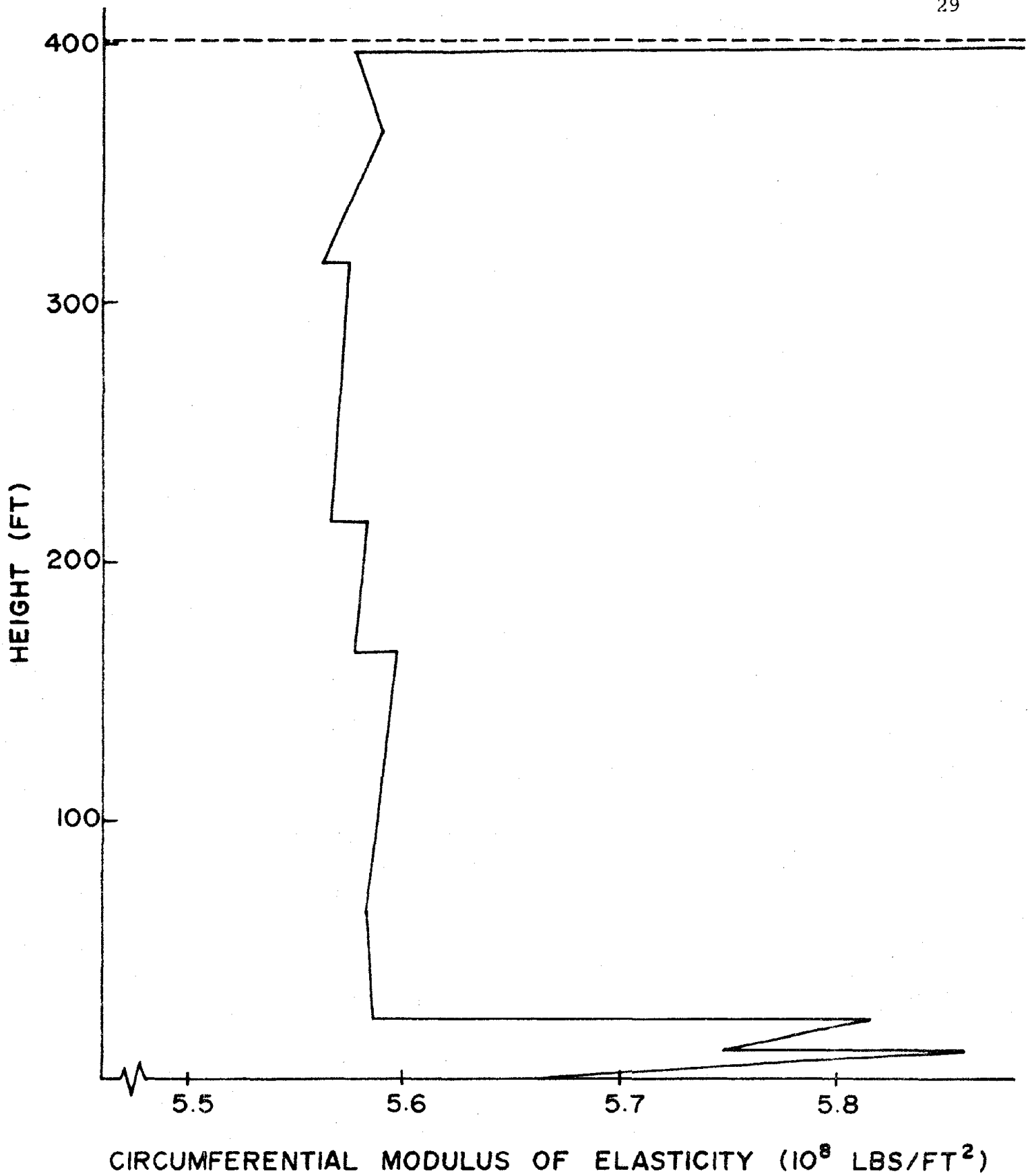


Fig. 2. The Distribution of Equivalent Modulus of Elasticity for the Circumferential Reinforcements Along the Meridional Direction.

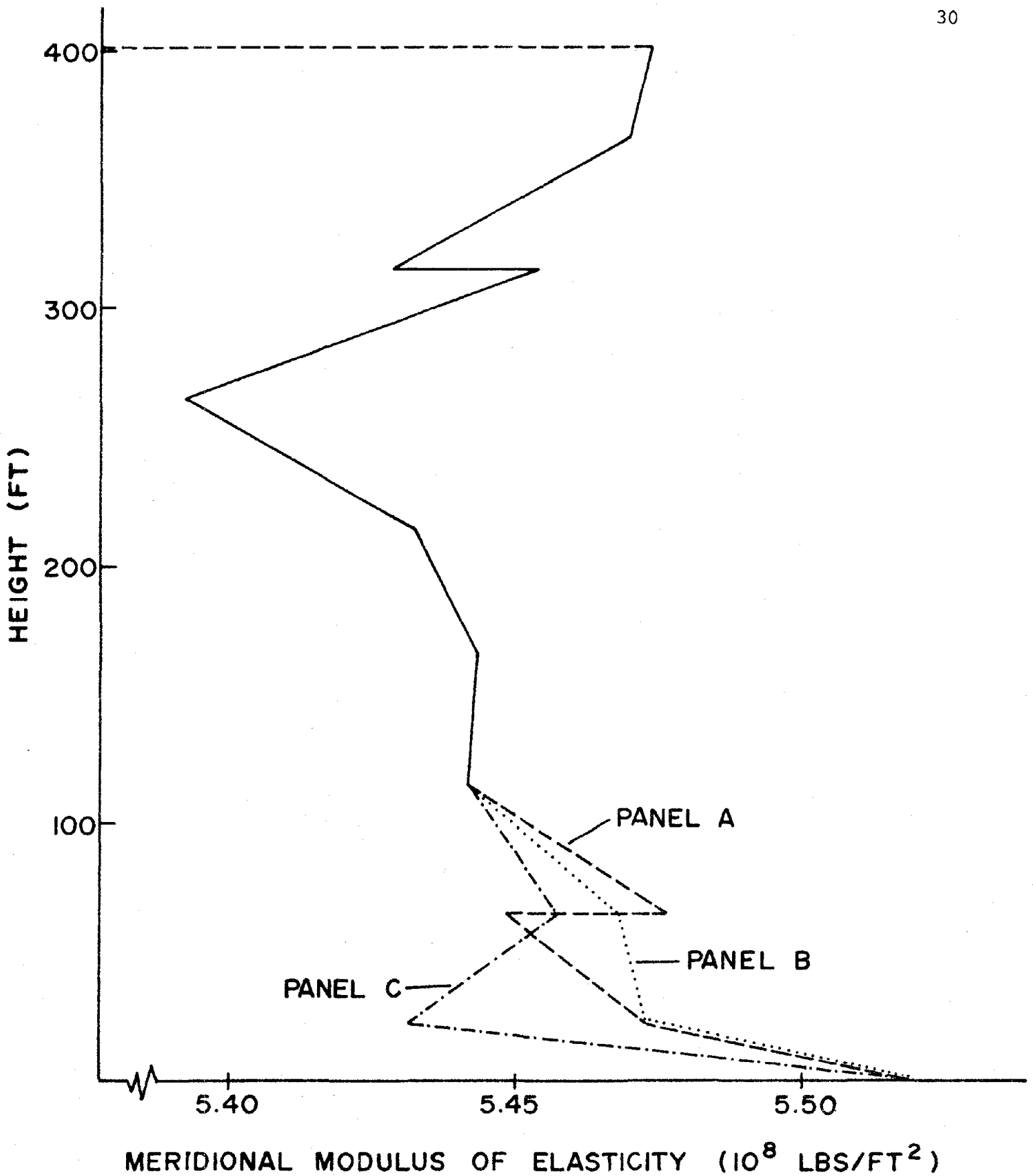


Fig. 3. The Distribution of Equivalent Modulus of Elasticity for the Meridional Reinforcements Along the Meridional Direction.

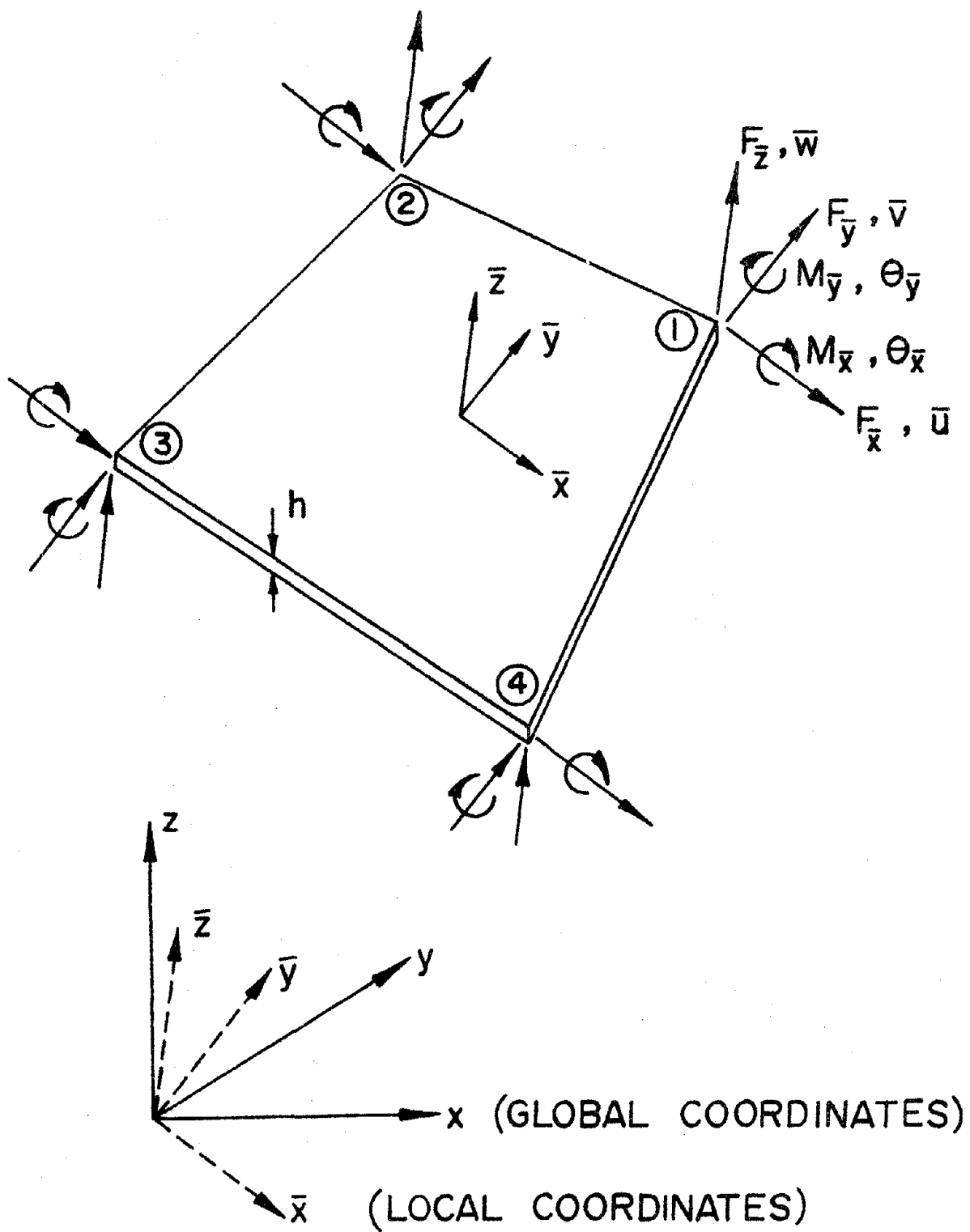


Fig. 4. A Quadrilateral Plate Finite Element in the Three-Dimensional Space.

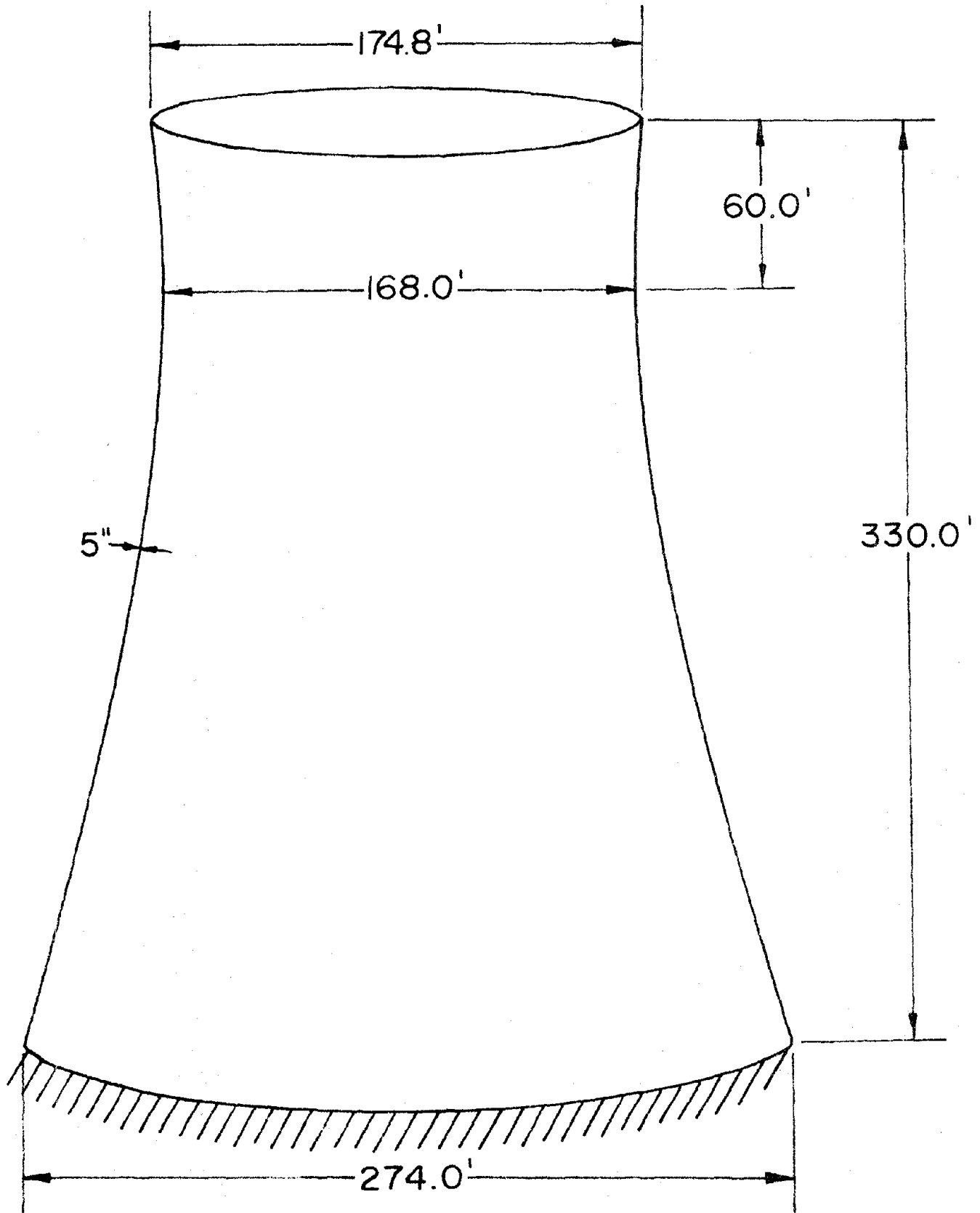


Fig. 5. An Example of a Reinforced Concrete Cooling Tower with Base Fixed.

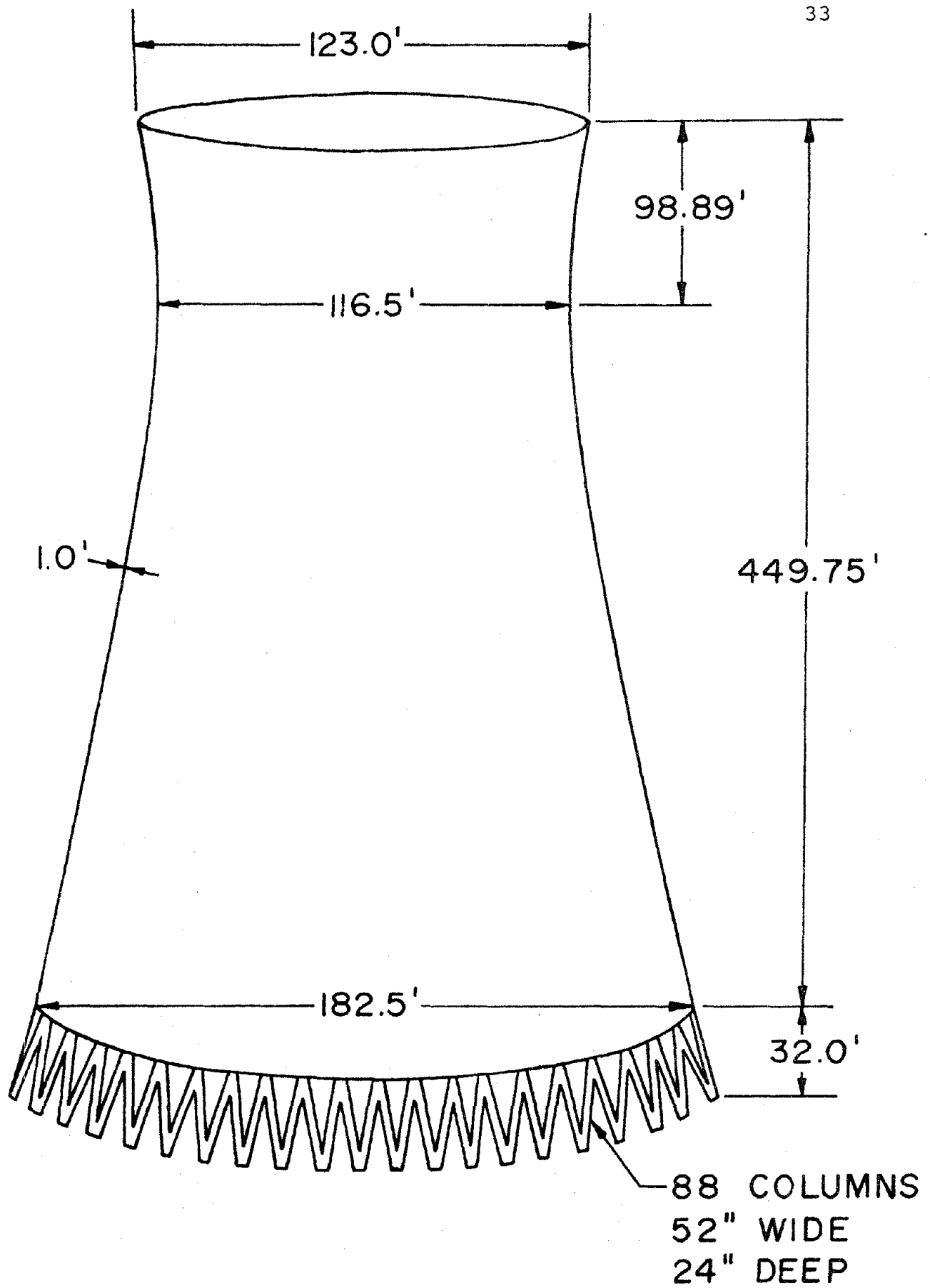


Fig. 6. An Example of a Reinforced Concrete Cooling Tower with Discrete Column Supports.

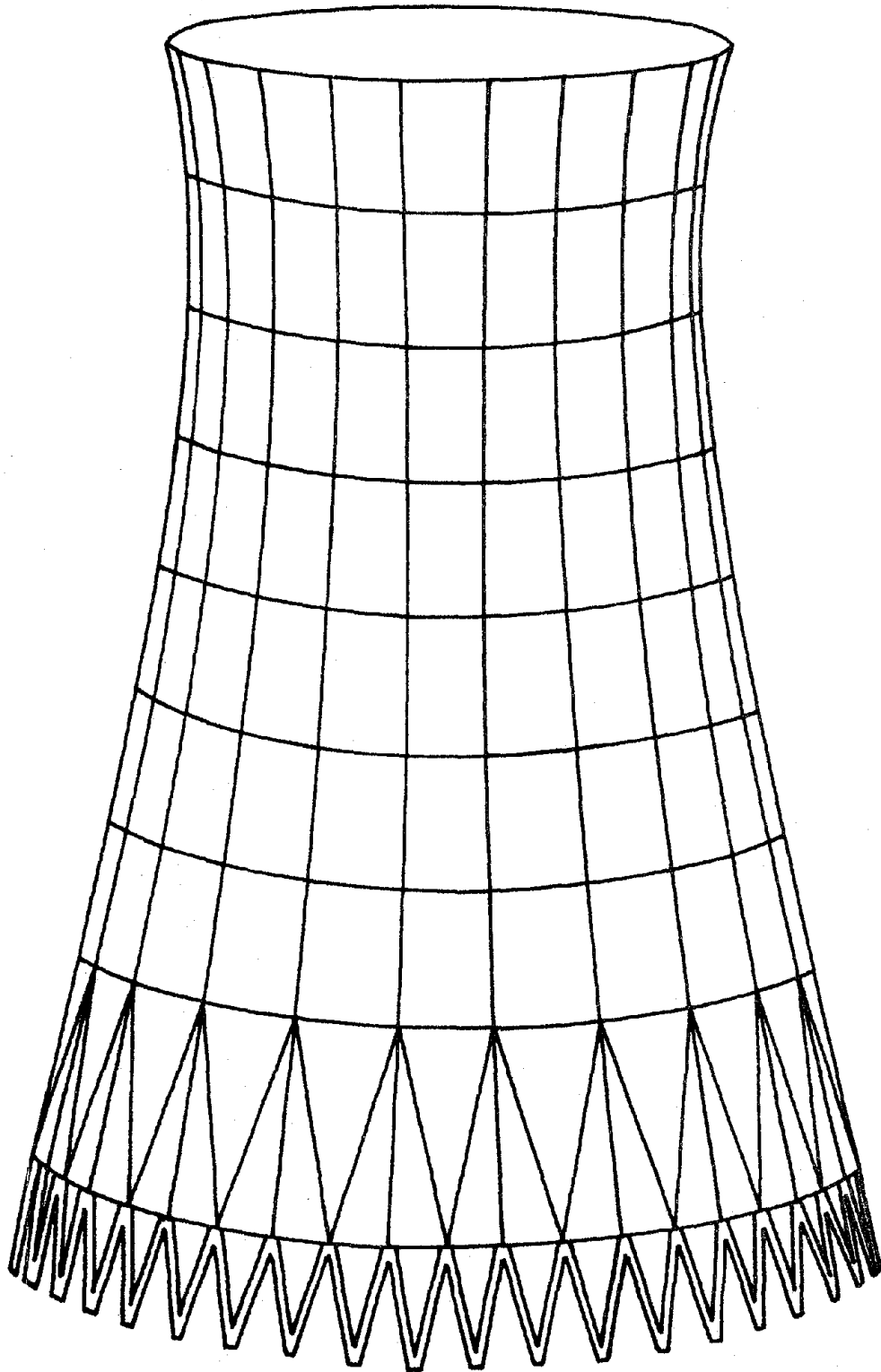


Fig. 7. The Finite Element Modeling of the Example Cooling Tower with Column Supports.

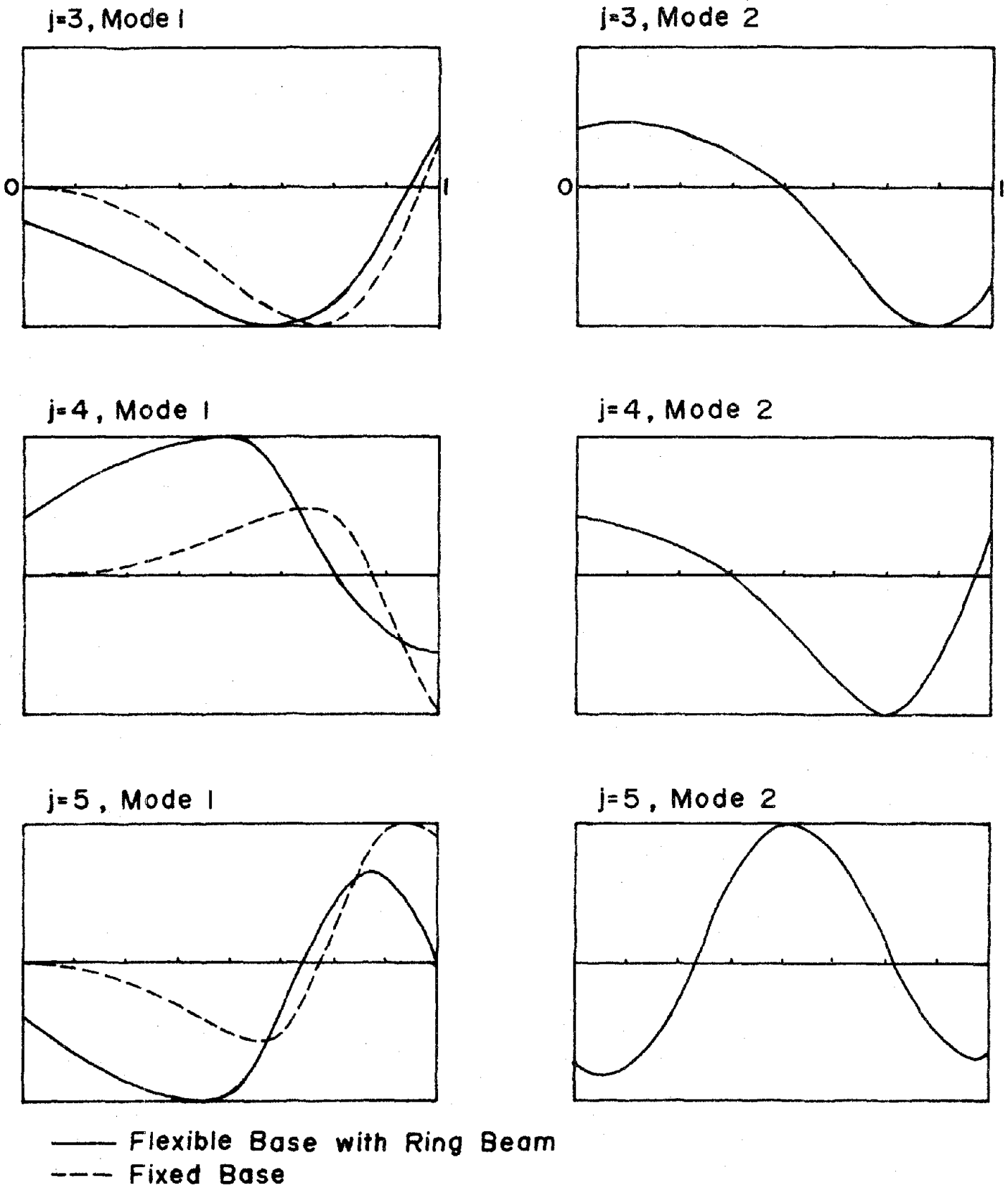


Fig. 8. The Longitudinal Mode Shapes for the Paradise Cooling Tower with Discrete Supporting Columns and Top Ring Beam (j = Circumferential Mode Number).

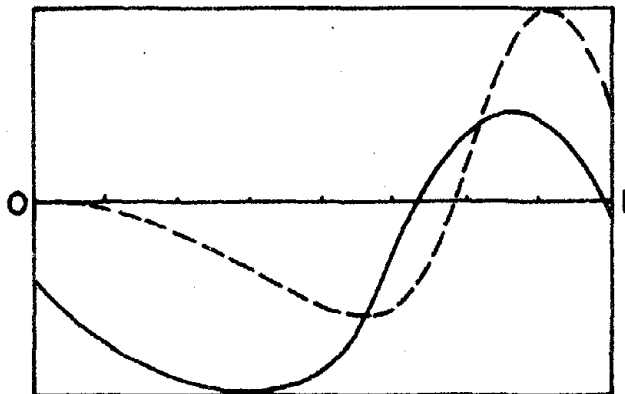
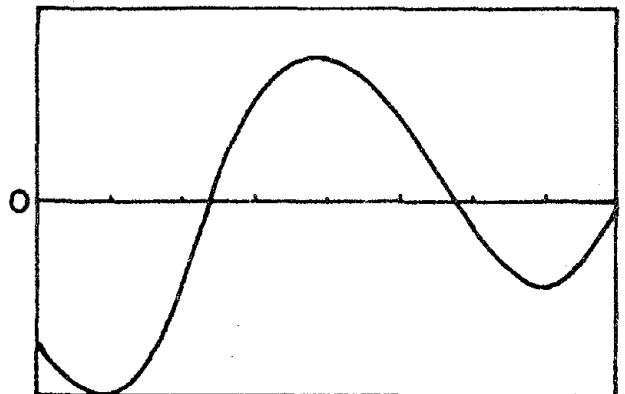
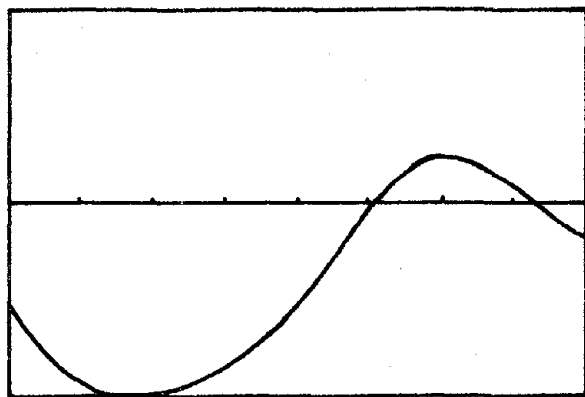
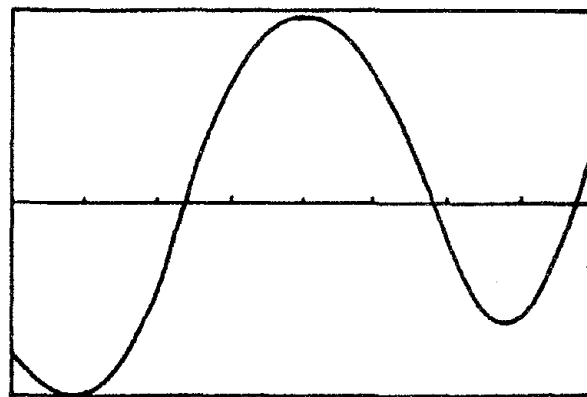
$j=6$, Mode 1 $j=6$, Mode 2 $j=7$, Mode 1 $j=7$, Mode 2

Fig. 8a. Continuation of Fig. 8.

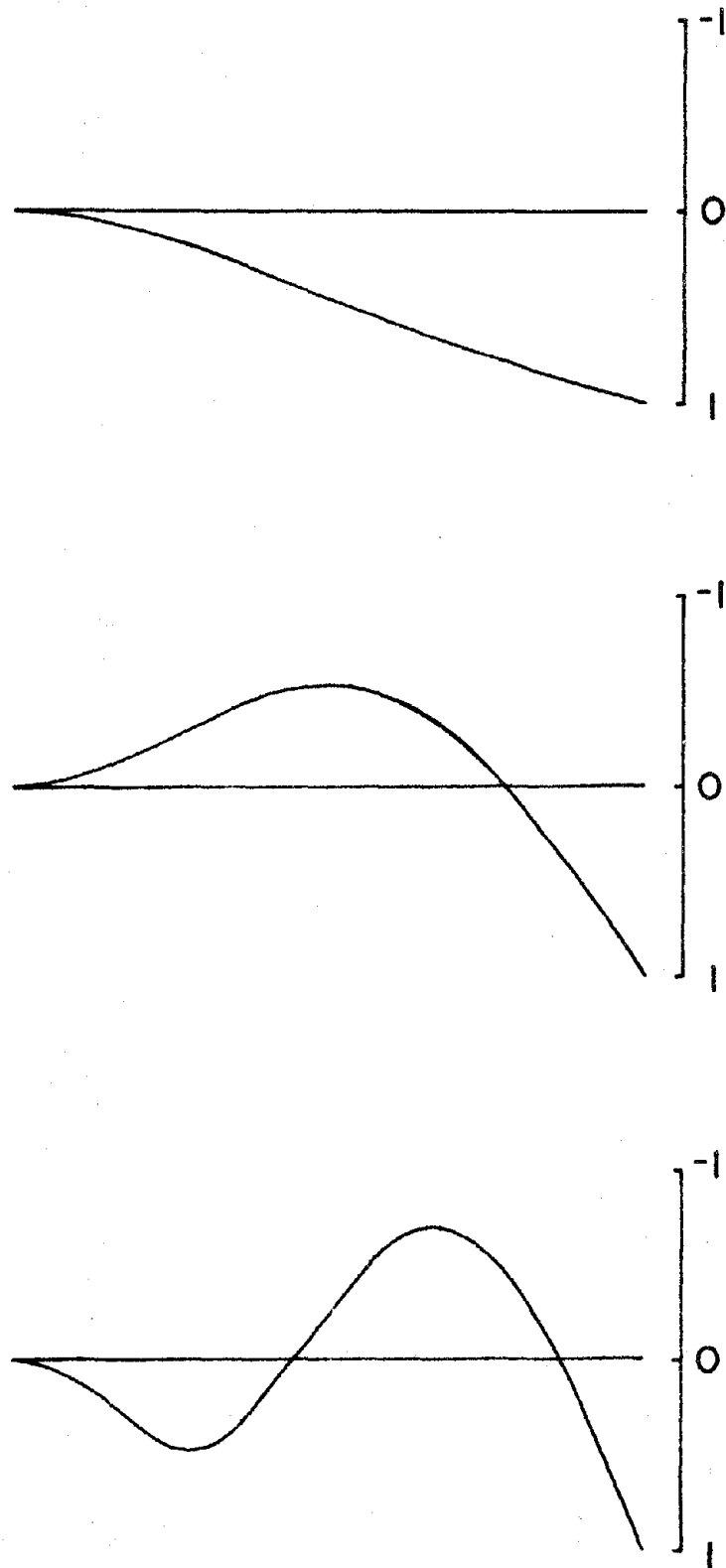


Fig. 9. The First Three Longitudinal Mode Shapes (with One Circumferential Wave) for the Cooling Tower Example (Fig. 5).

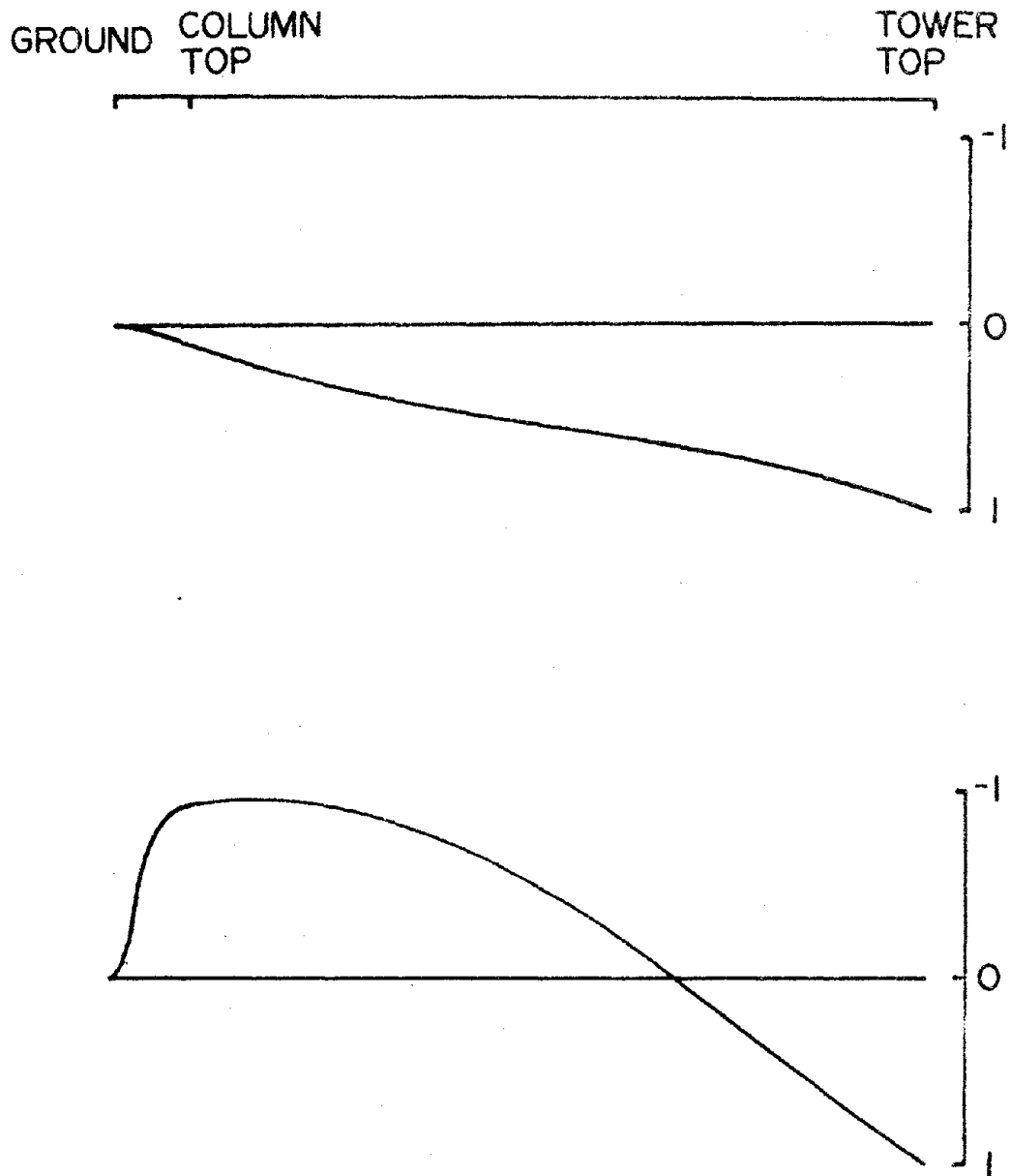


Fig. 10. The First Two Longitudinal Mode Shapes (with One Circumferential Wave) for the Paradise Cooling Tower.

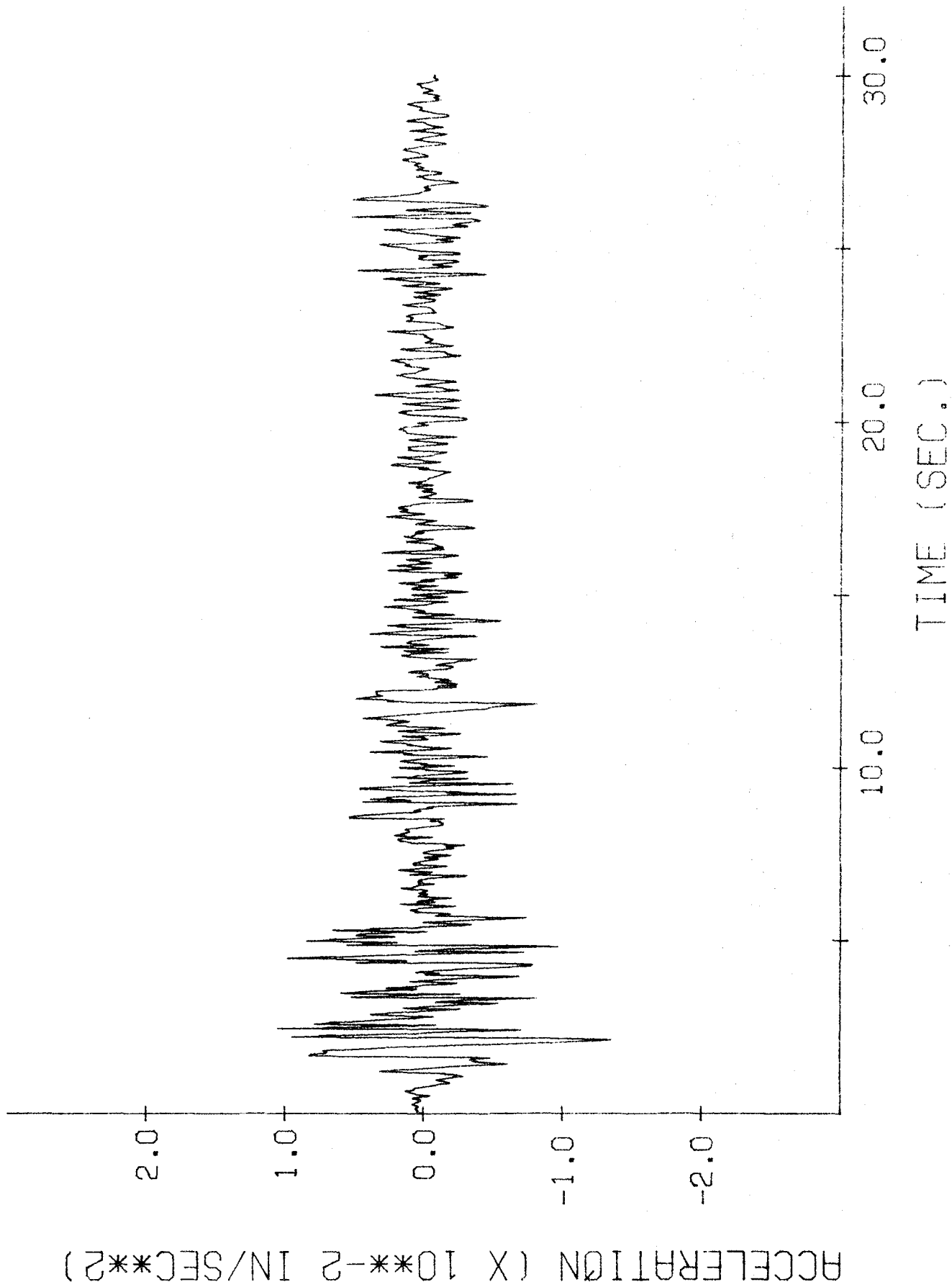


Fig. 11. The South-North Acceleration Component of the El Centro Earthquake in 1940.

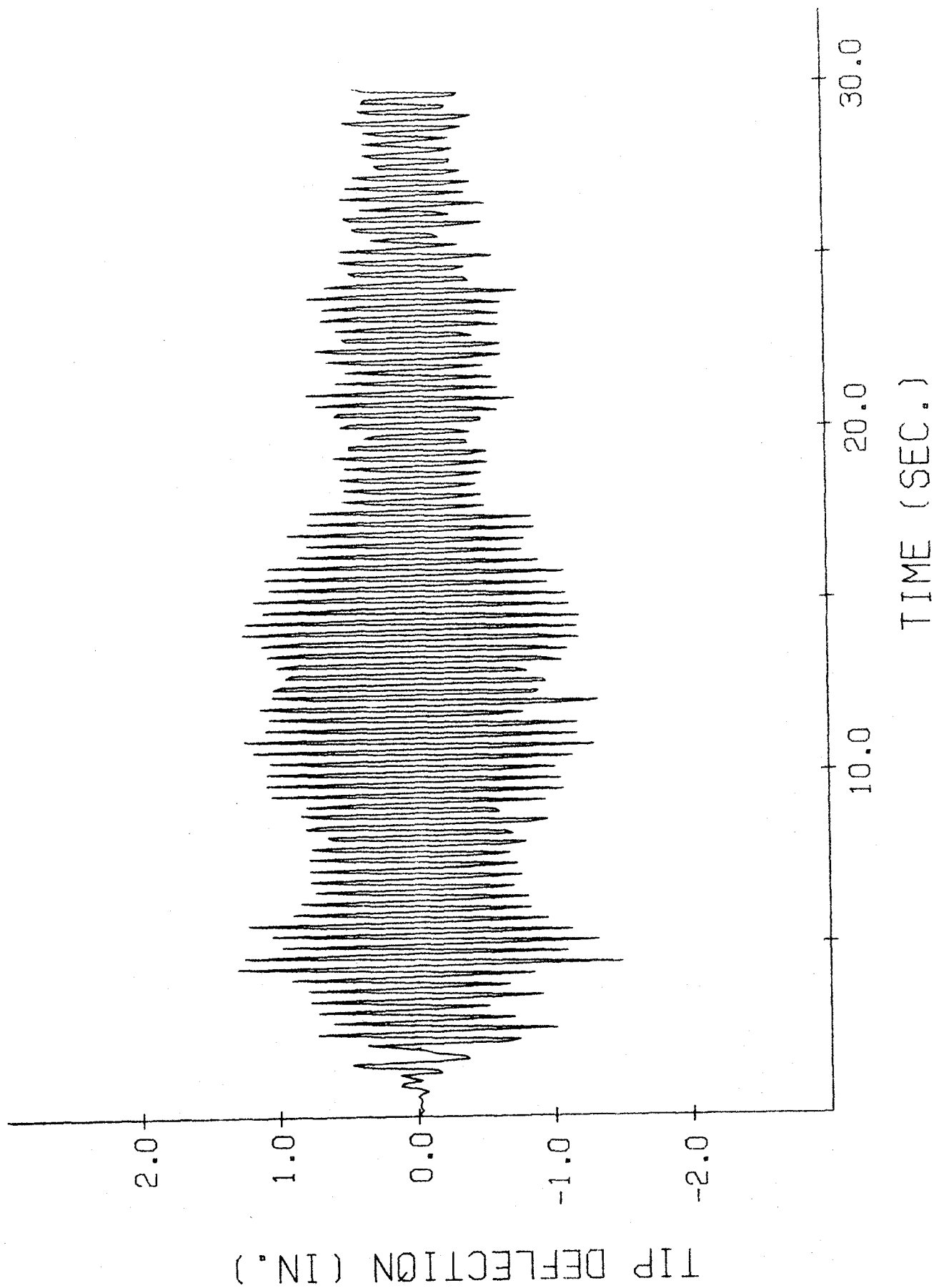


Fig. 12. Time-History Response of Tip Deflection at $\theta=0^\circ$ for the Example Cooling Tower with Fixed Base.

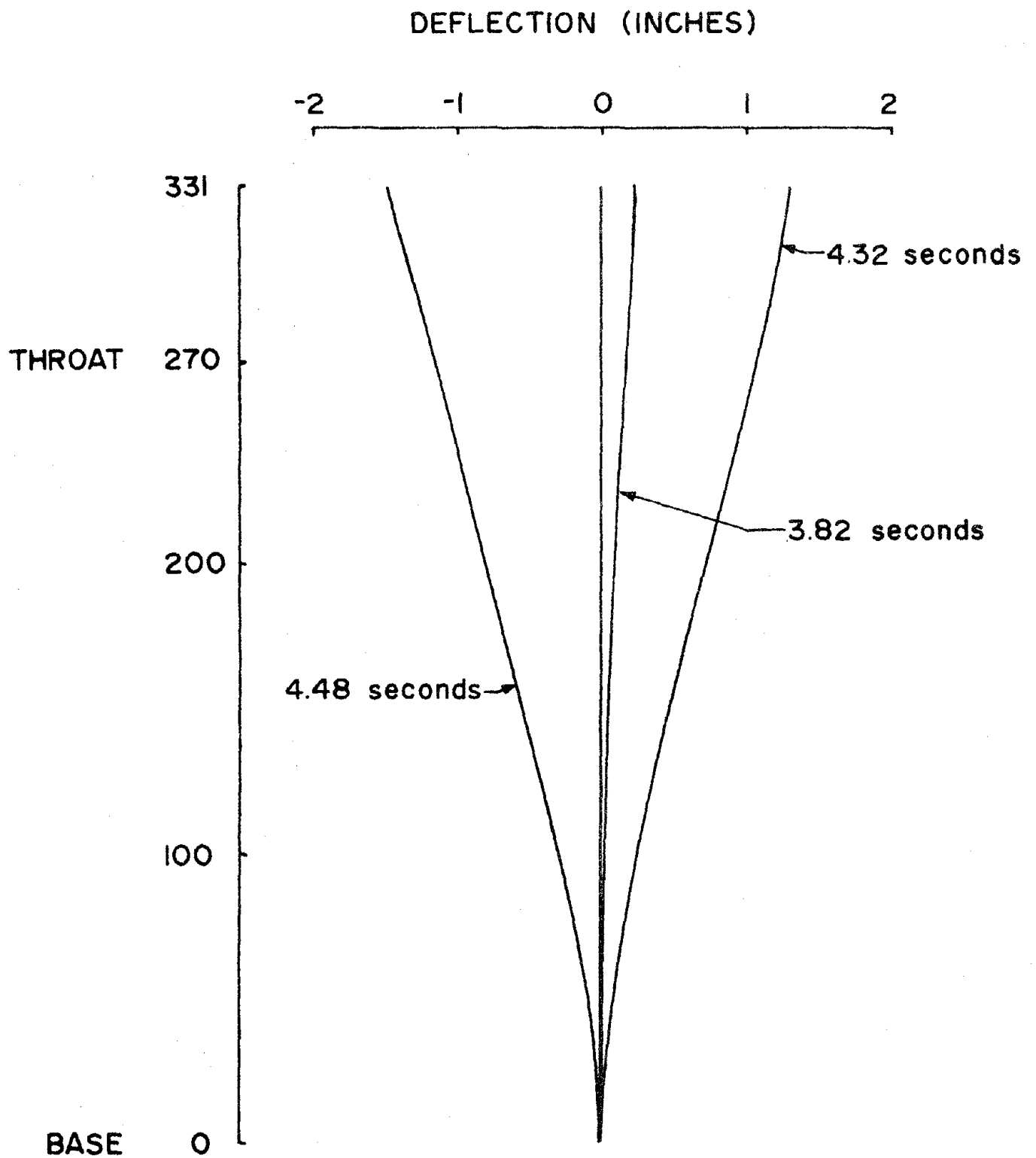


Fig. 13. Longitudinal Distribution of Deflection Shapes at $\theta=0^\circ$ for the Example Cooling Tower with Fixed Base.

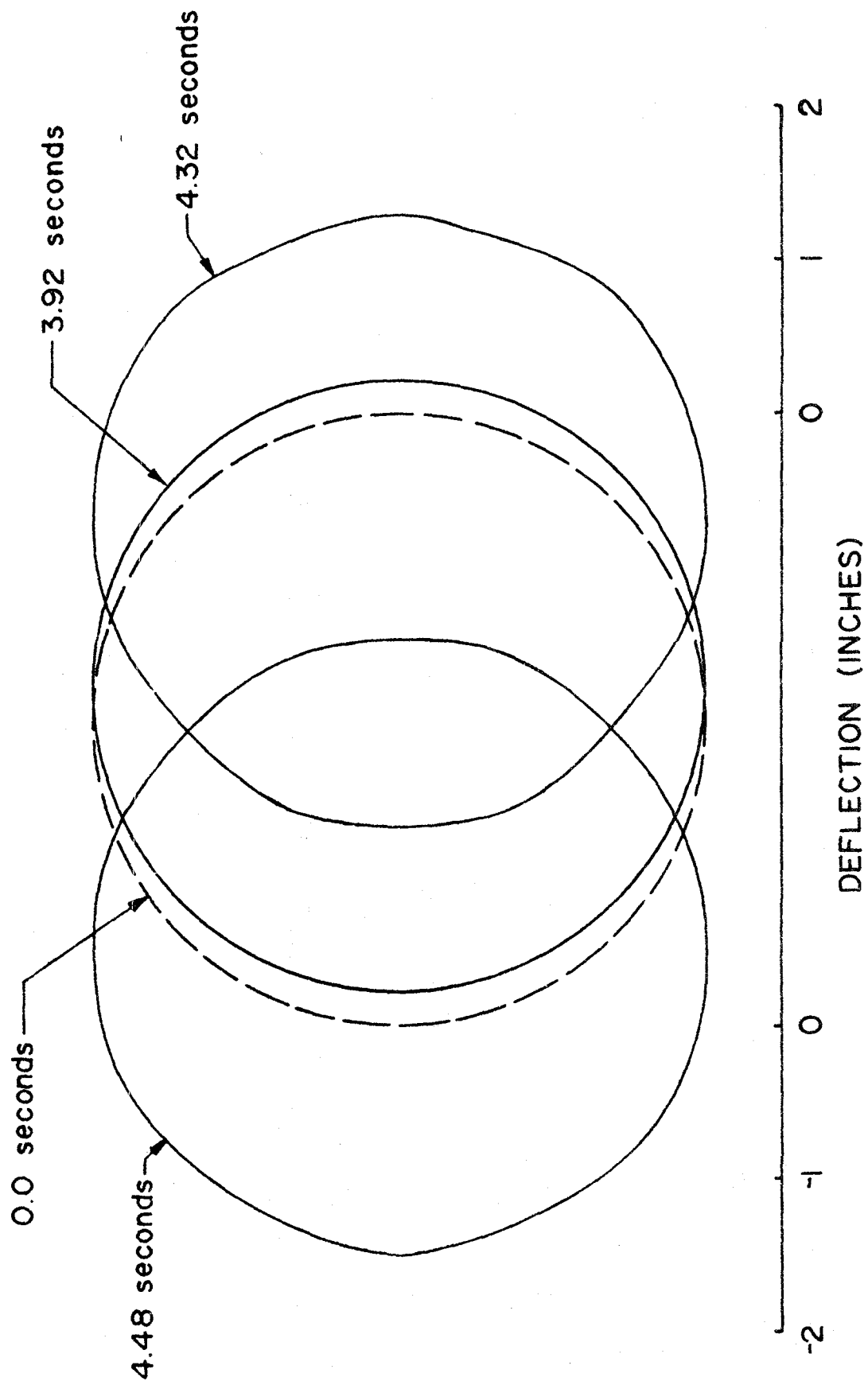


Fig. 14. Circumferential Deflection Shapes at the Top of the Example Cooling Tower with Fixed Base.

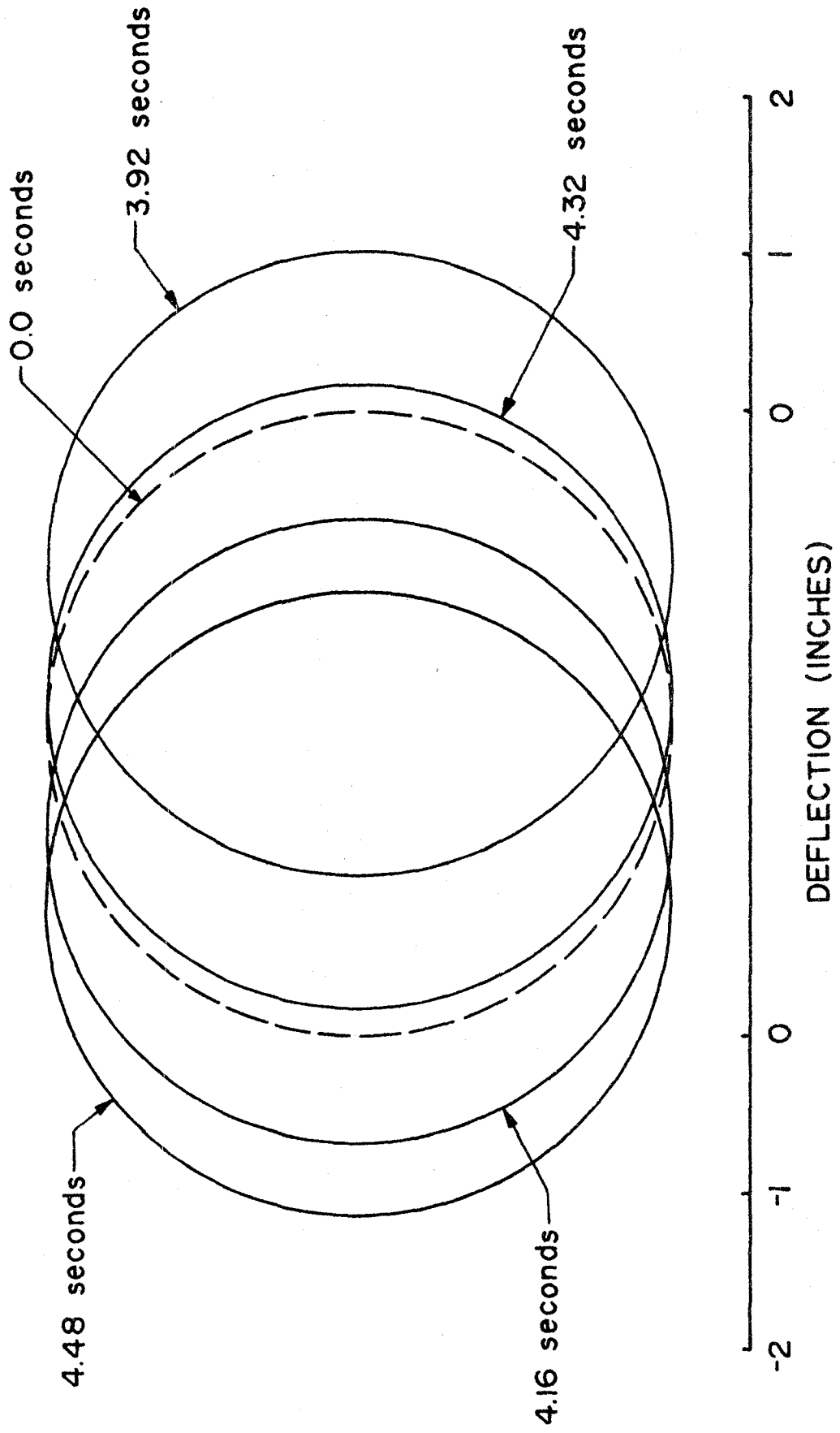


Fig. 15. Circumferential Deflection Shapes at the Throat of the Example Cooling Tower with Fixed Base.

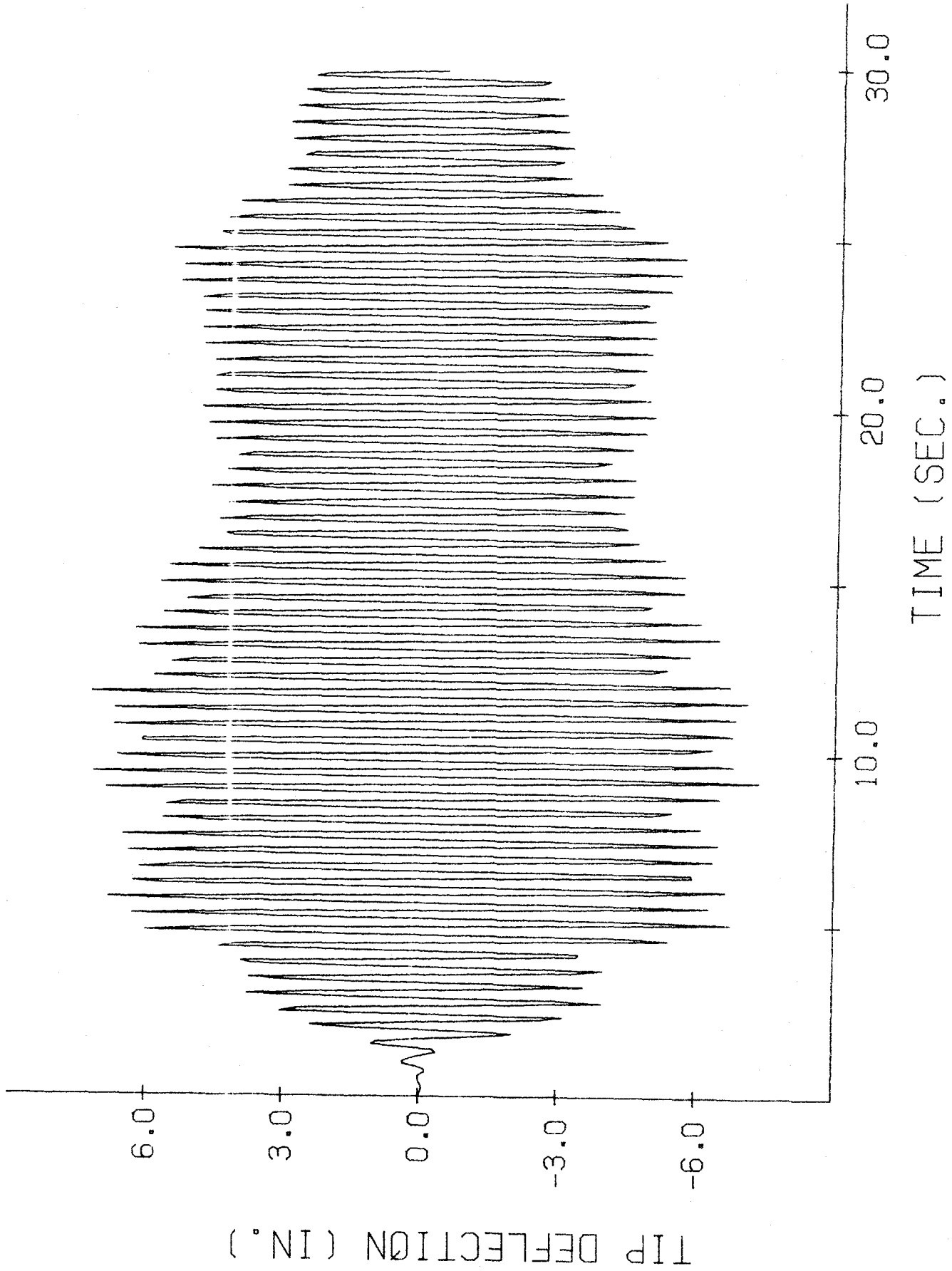


Fig. 16. Time-History Response of Tip Deflection at $\theta=0^\circ$ for the Paradise Cooling Tower.

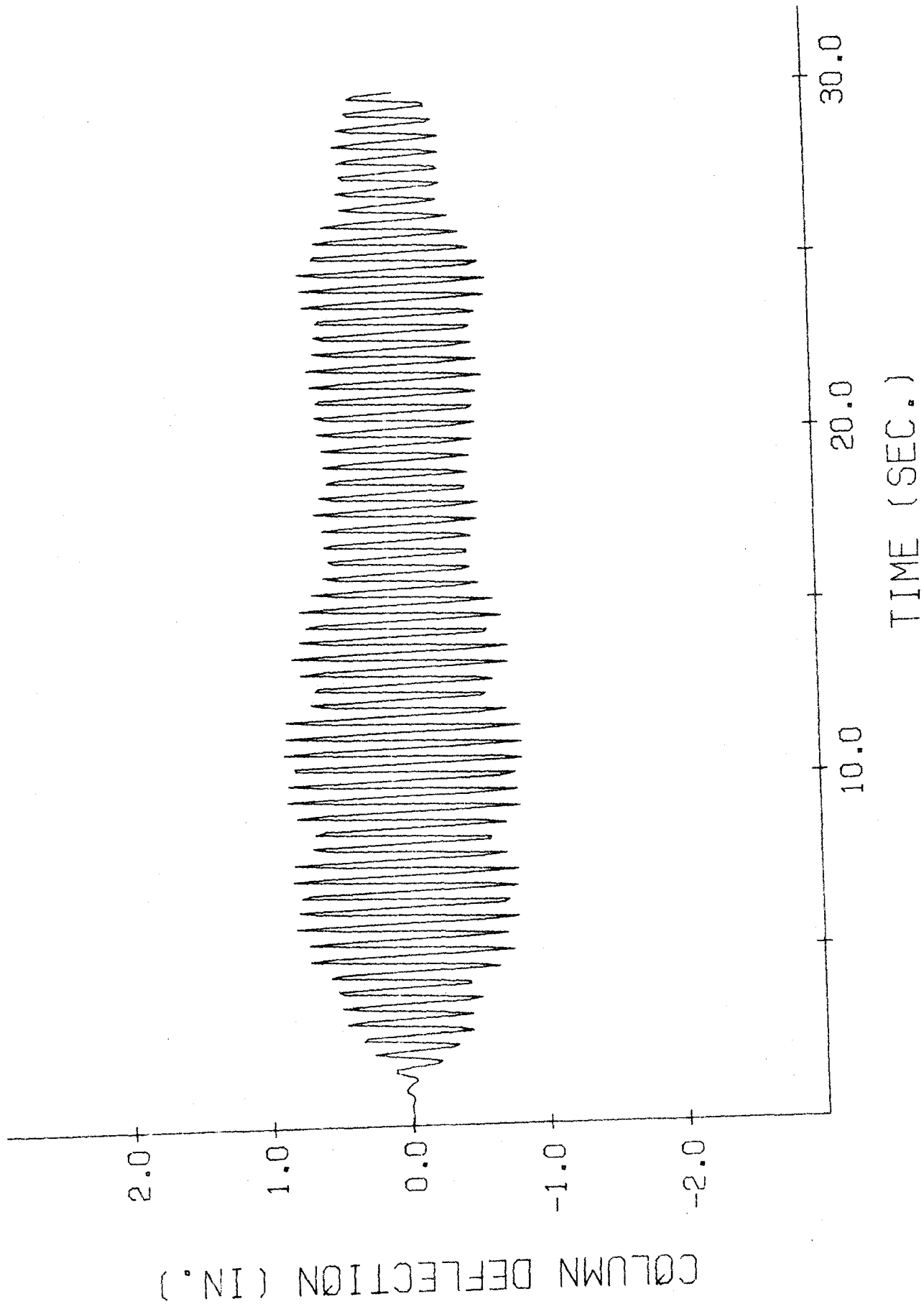


Fig. 17. Time-History Response of Deflection at the Top of the Column at $\theta=0^\circ$ for the Paradise Cooling Tower.

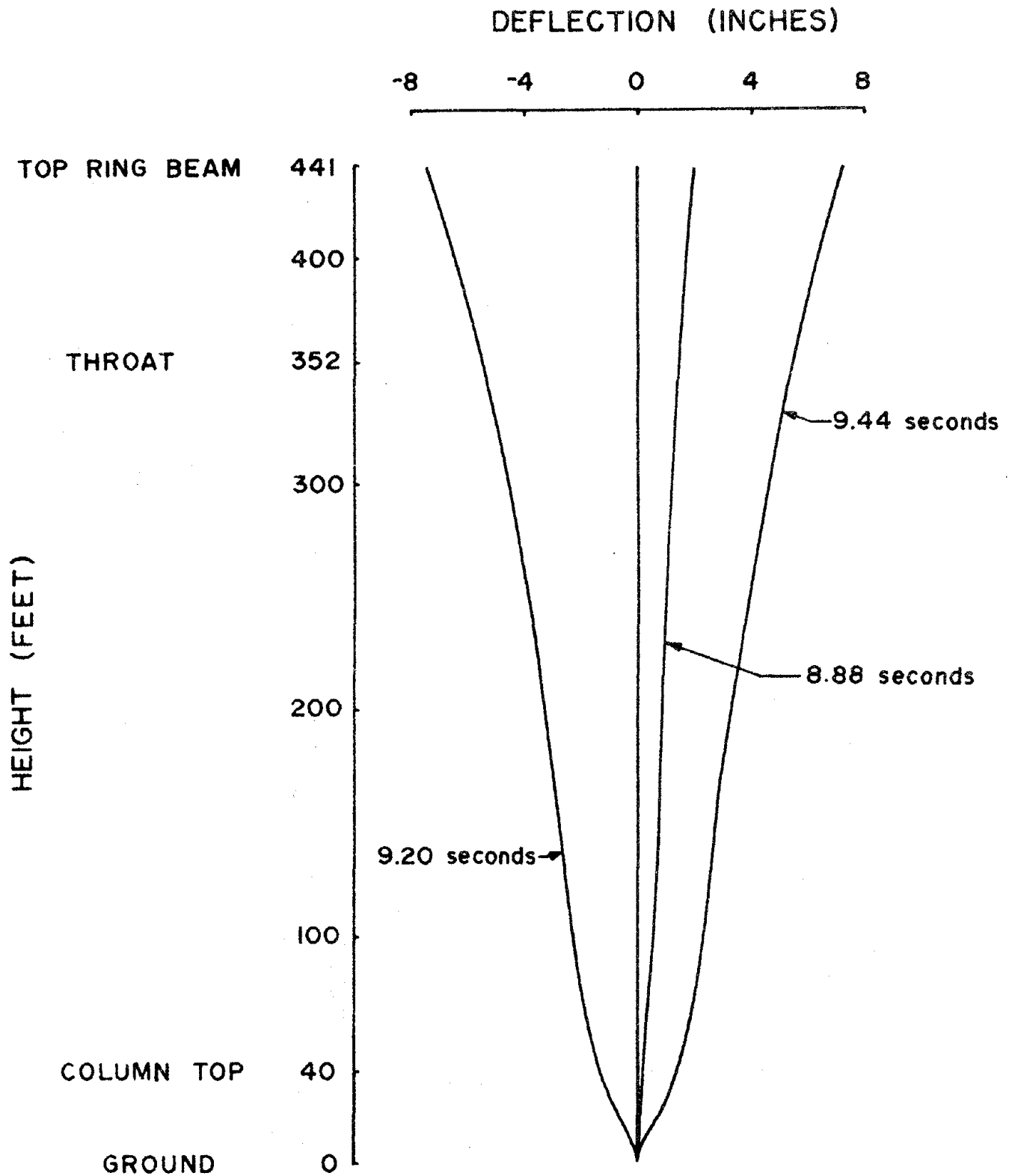


Fig. 18. Longitudinal Distribution of Deflection Shapes at $\theta=0^\circ$ for the Paradise Cooling Tower.

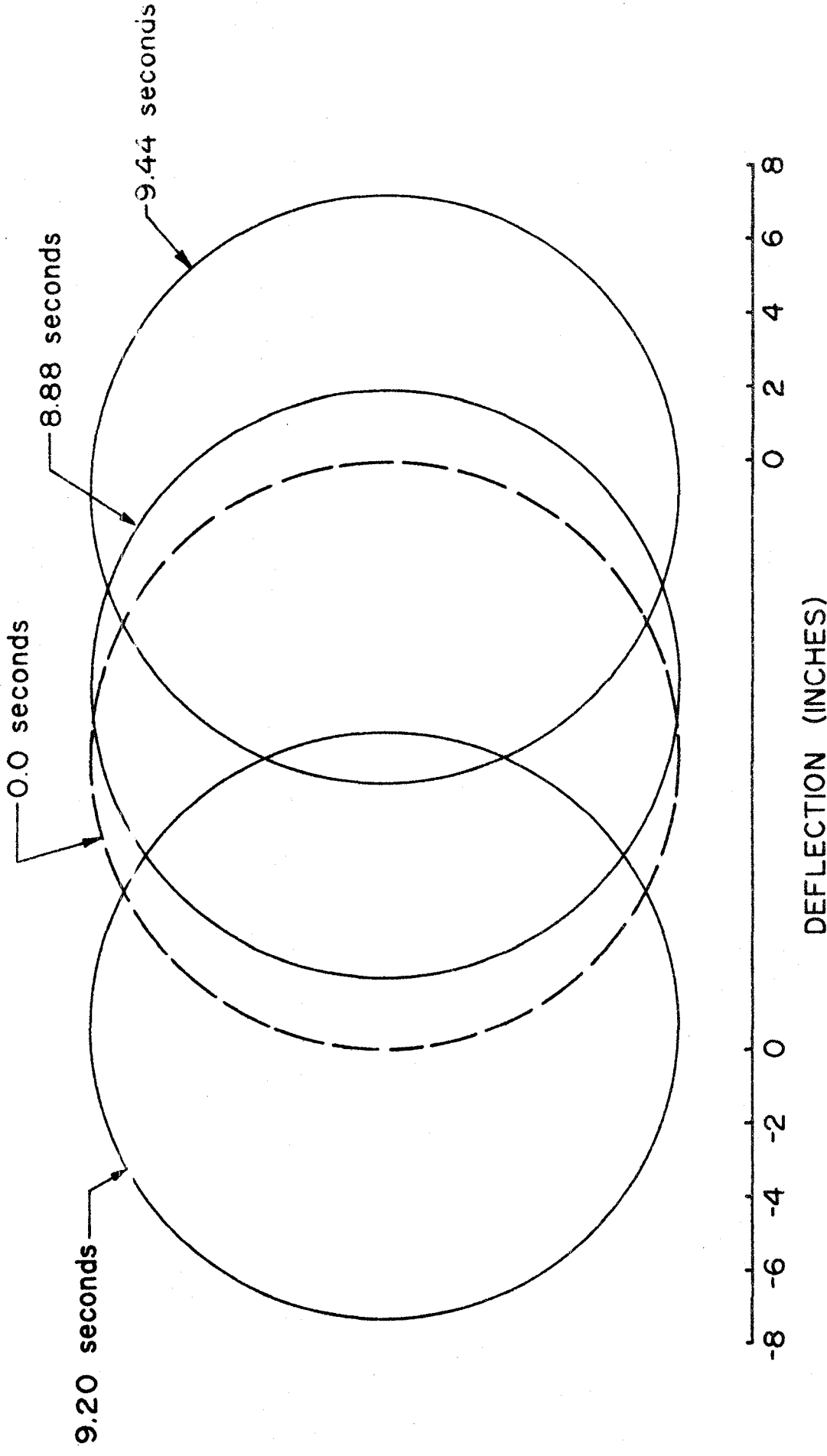


Fig. 19. Circumferential Deflection Shapes at the Top of the Paradise Cooling Tower.

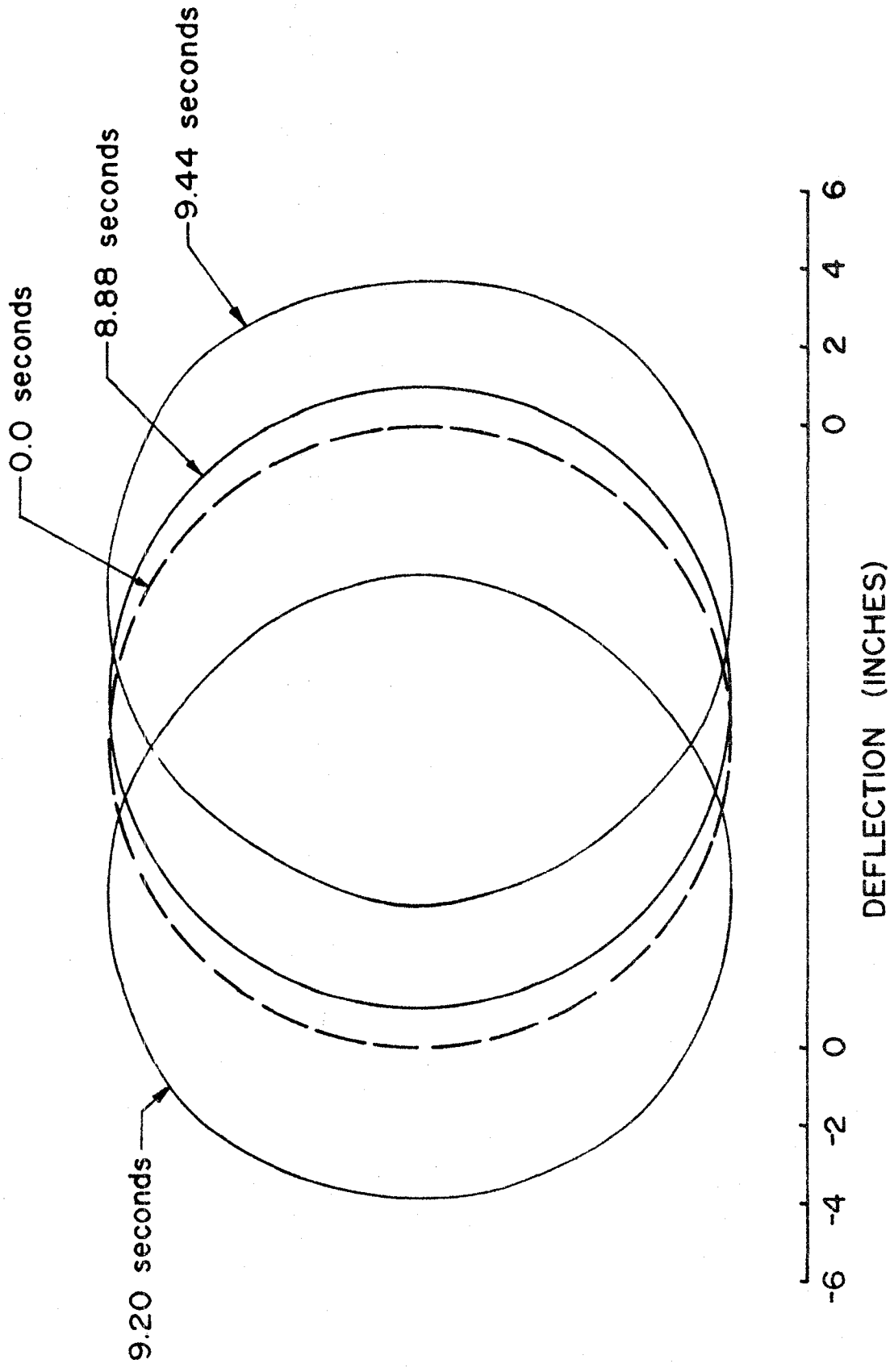


Fig. 20. Circumferential Deflection Shapes of the Paradise Cooling Tower at 240 Feet Above Ground.

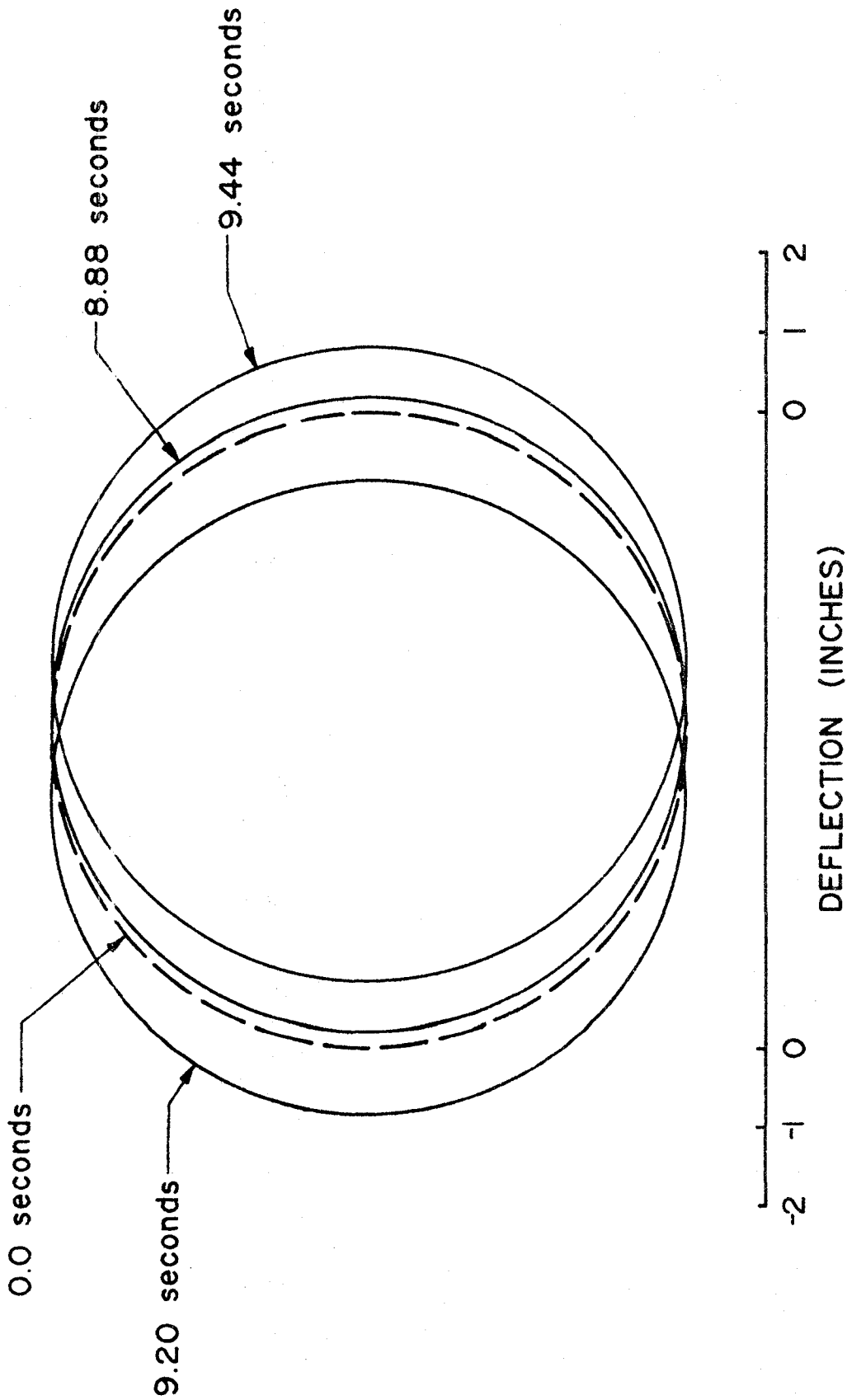


Fig. 21. Circumferential Deflection Shapes at the Base (Top of the Columns) of the Paradise Cooling Tower.

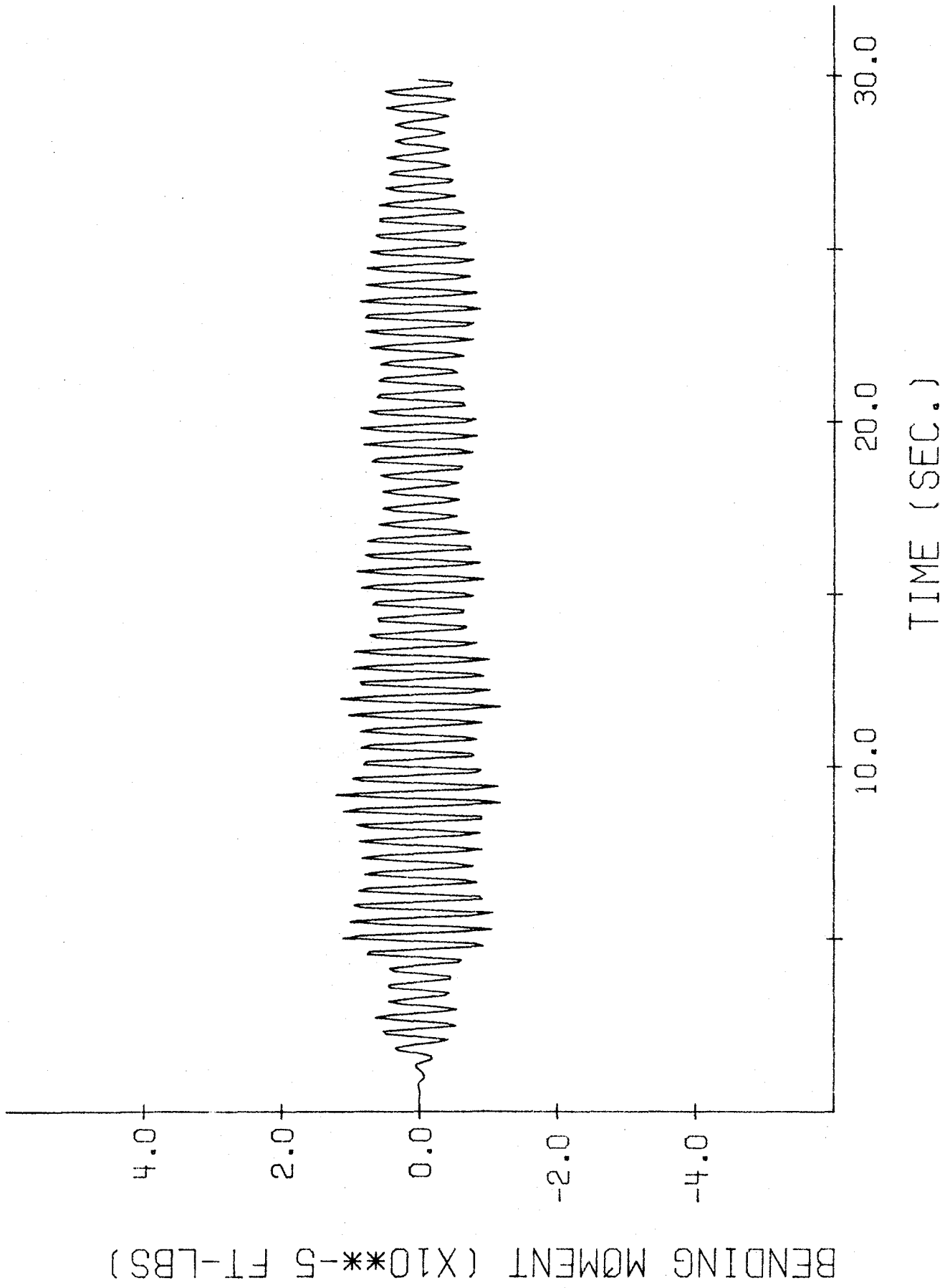


Fig. 22. Time-History Response of Bending Moment at Column Base at $\theta=5.6^\circ$ for the Paradise Cooling Tower.

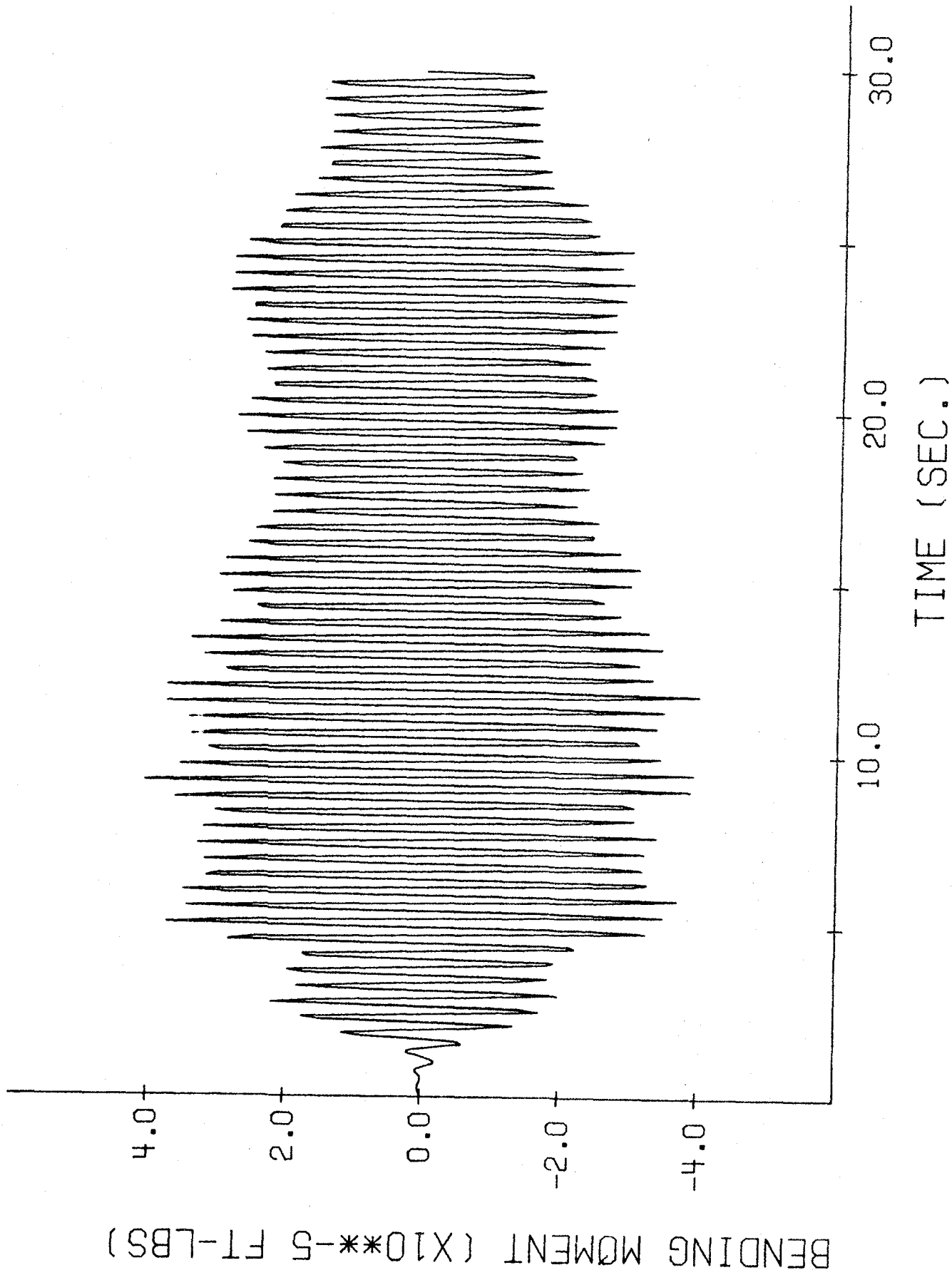


Fig. 23. Time-History Response of Bending Moment at Column Top at $\theta=0^\circ$ for the Paradise Cooling Tower.

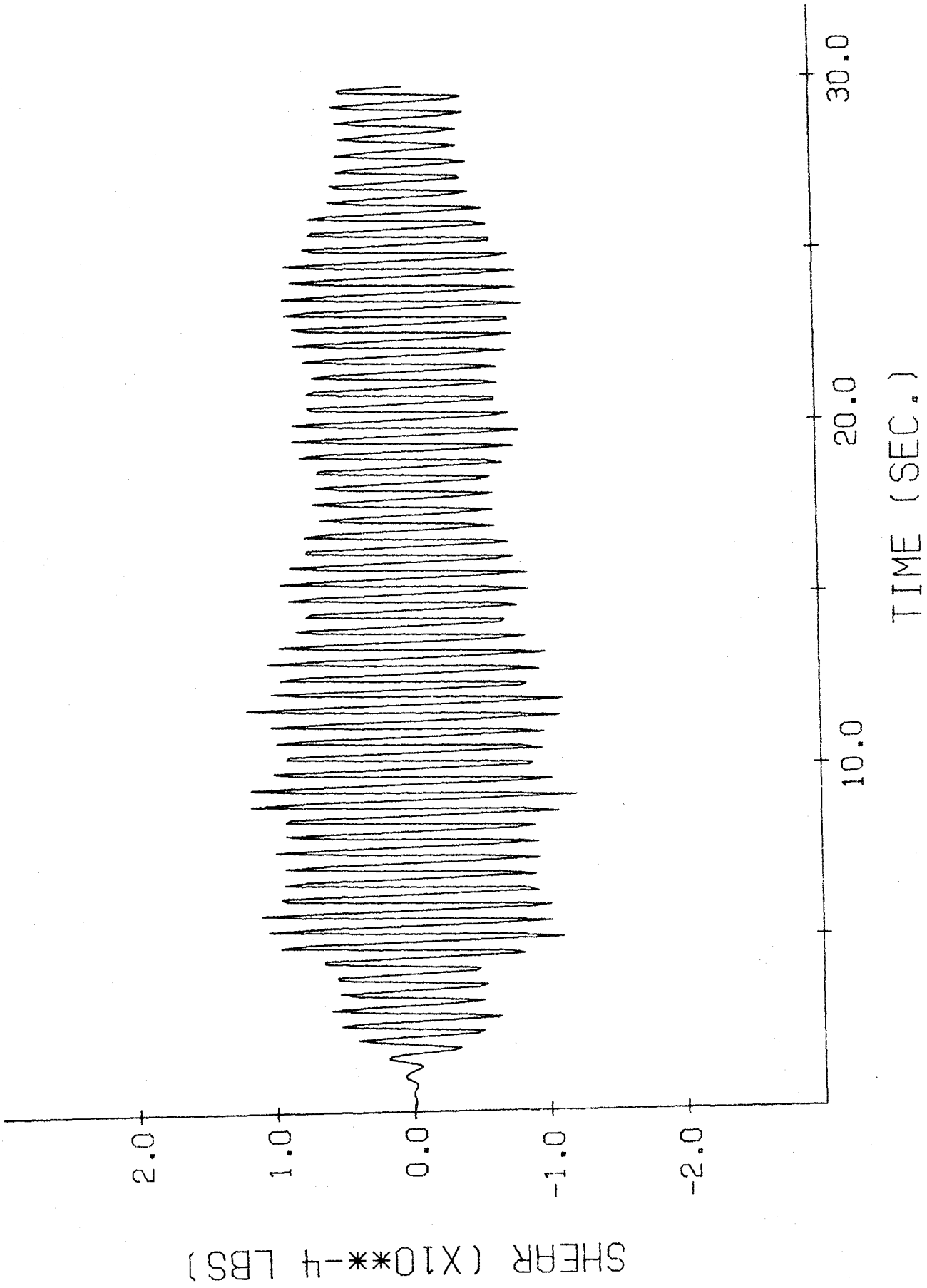


Fig. 24. Time-History Response of Shearing Force in the Column at $\theta=0^\circ$ for the Paradise Cooling Tower.

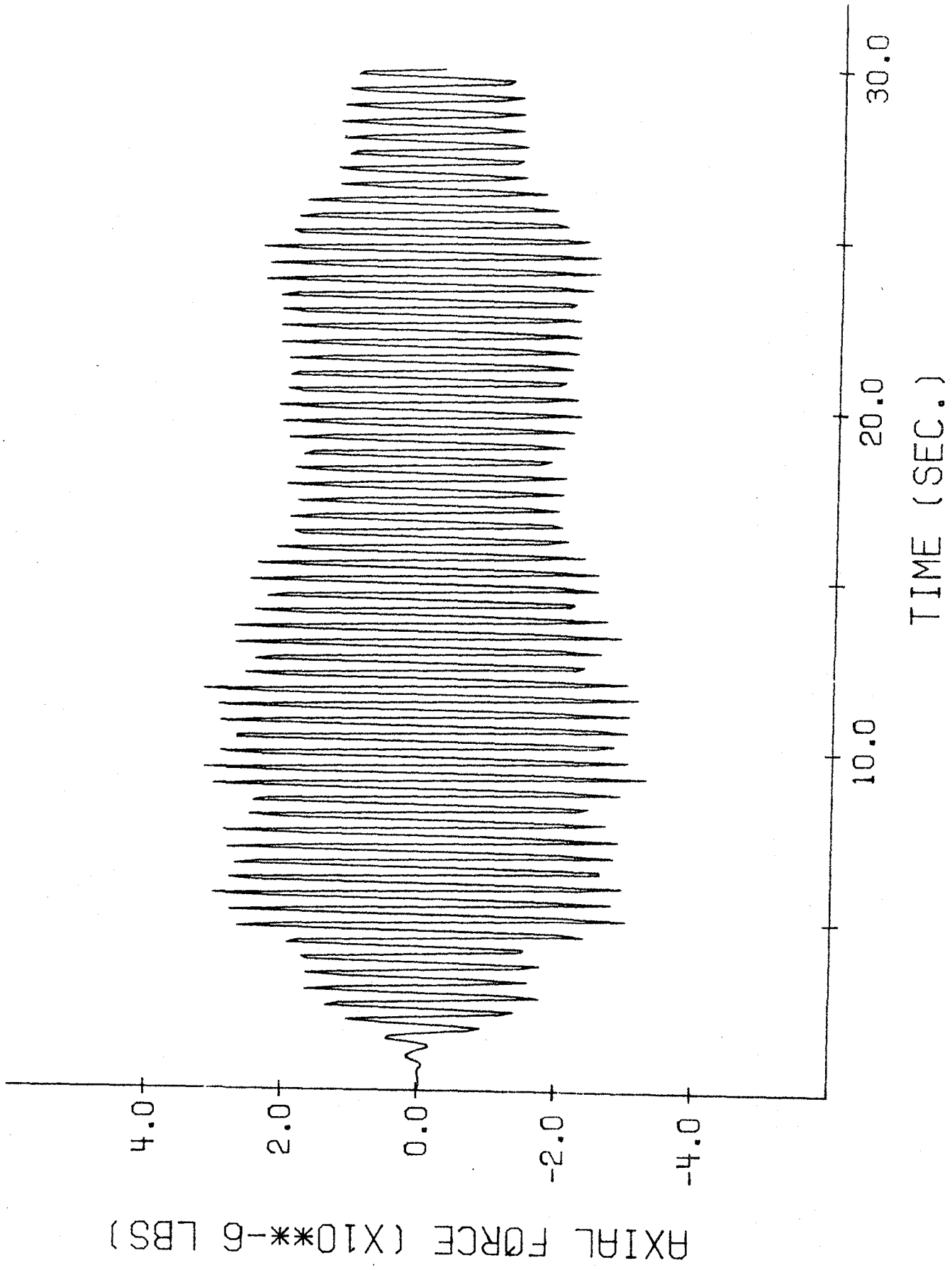


Fig. 25. Time-History Response of Axial Force in the Column at $\theta=0^\circ$ for the Paradise Cooling Tower.

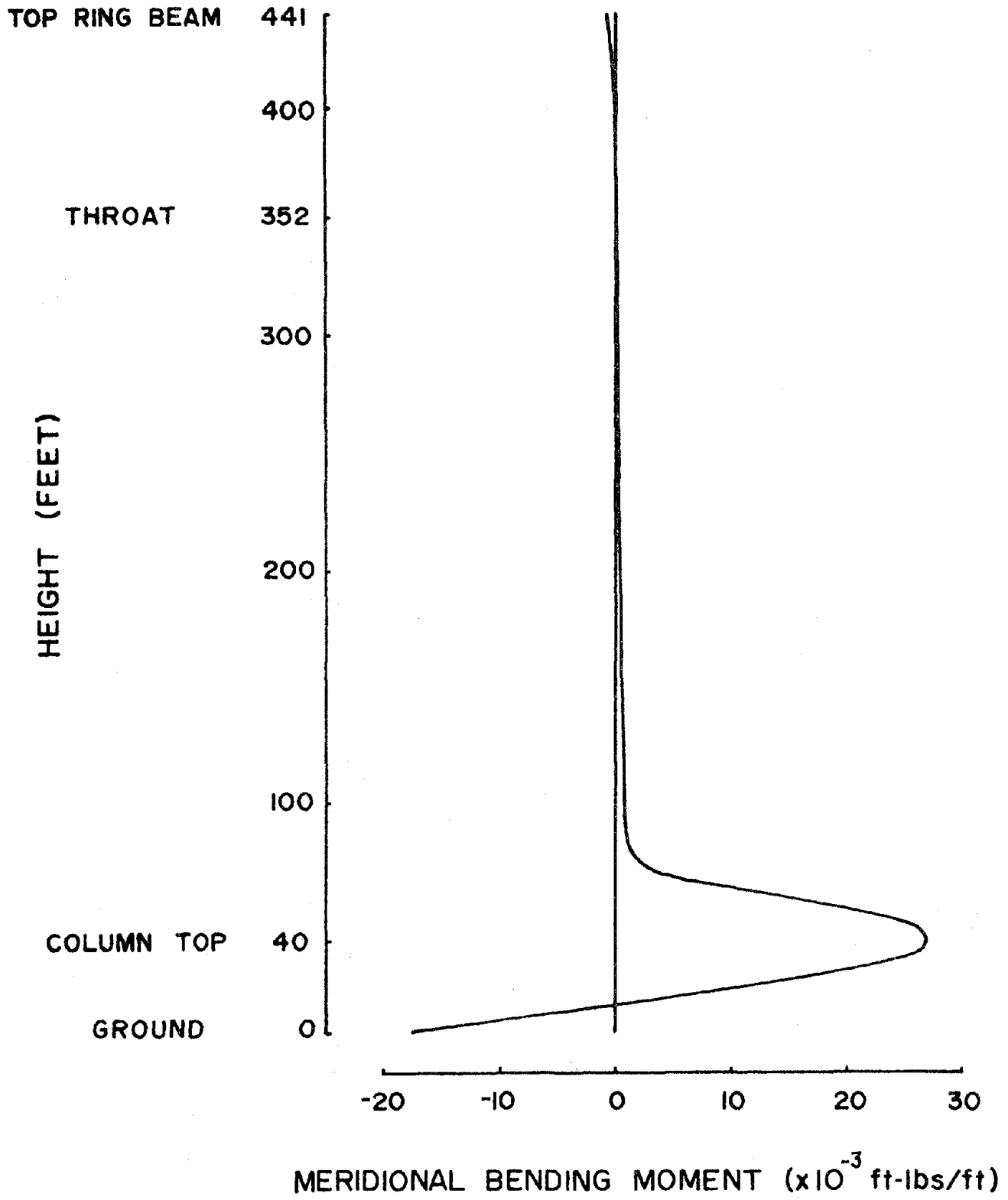


Fig. 26. Distribution of Meridional Bending Moment at $\theta=0^\circ$ for the Paradise Cooling Tower (at 9.2 Seconds).

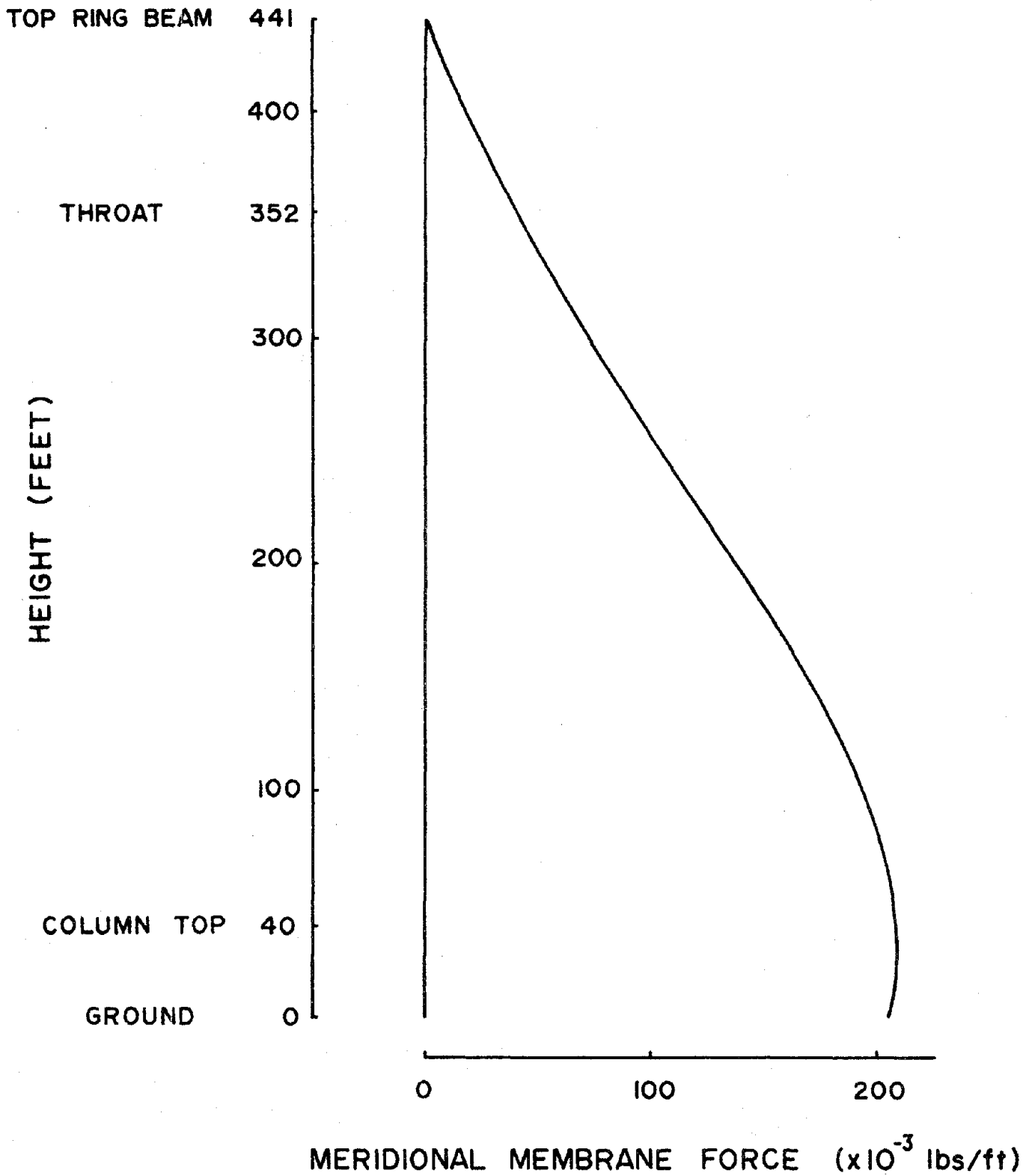


Fig. 27. Distribution of Meridional Membrane Force at $\theta=0^\circ$ for the Paradise Cooling Tower (at 9.2 Seconds).

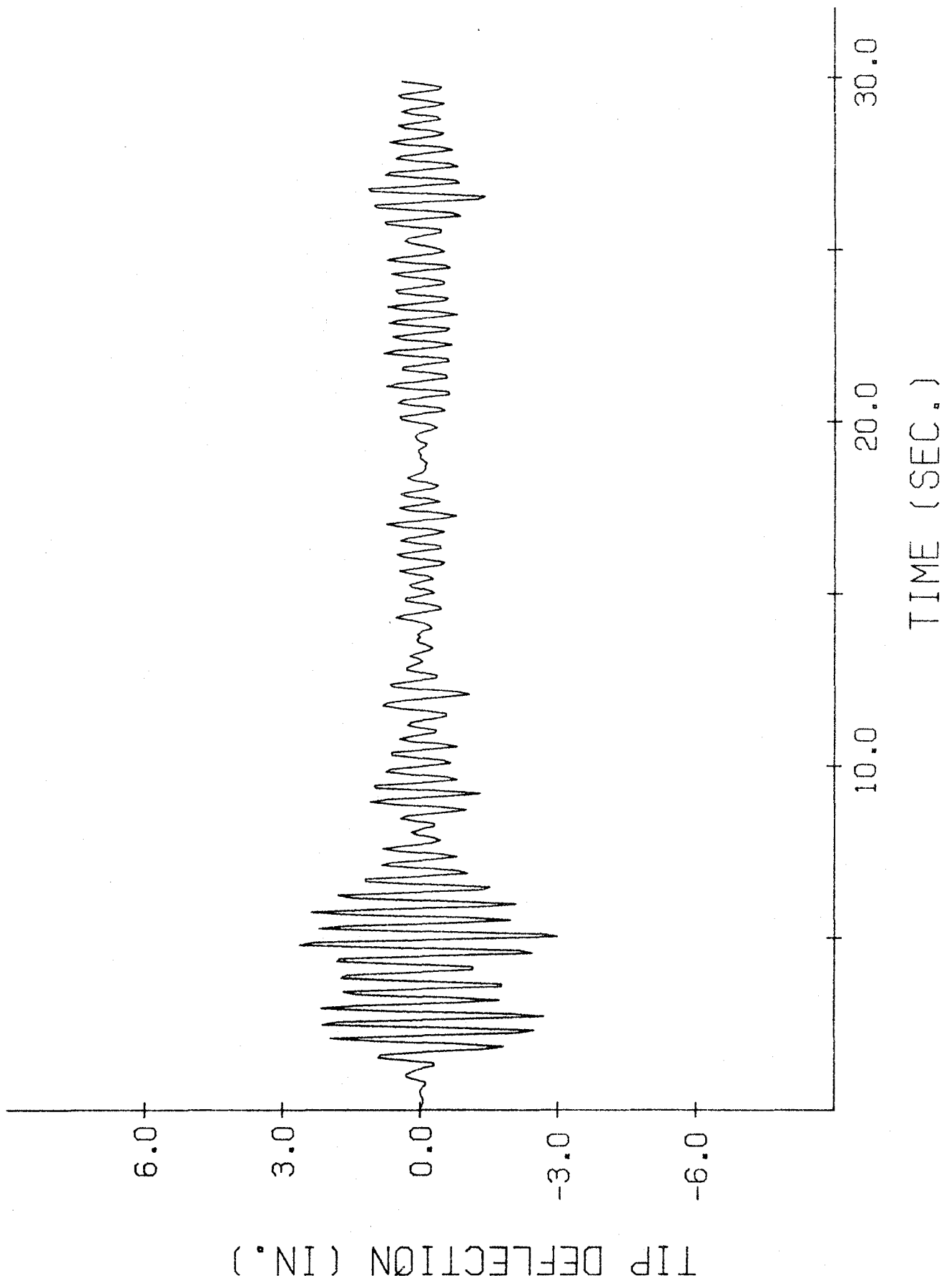


Fig. 28. Tip Deflection at $\theta=0^\circ$ vs. Time Curve for the Paradise Cooling Tower with Damping Coefficient Equal to 4 Percent of its Critical Value.

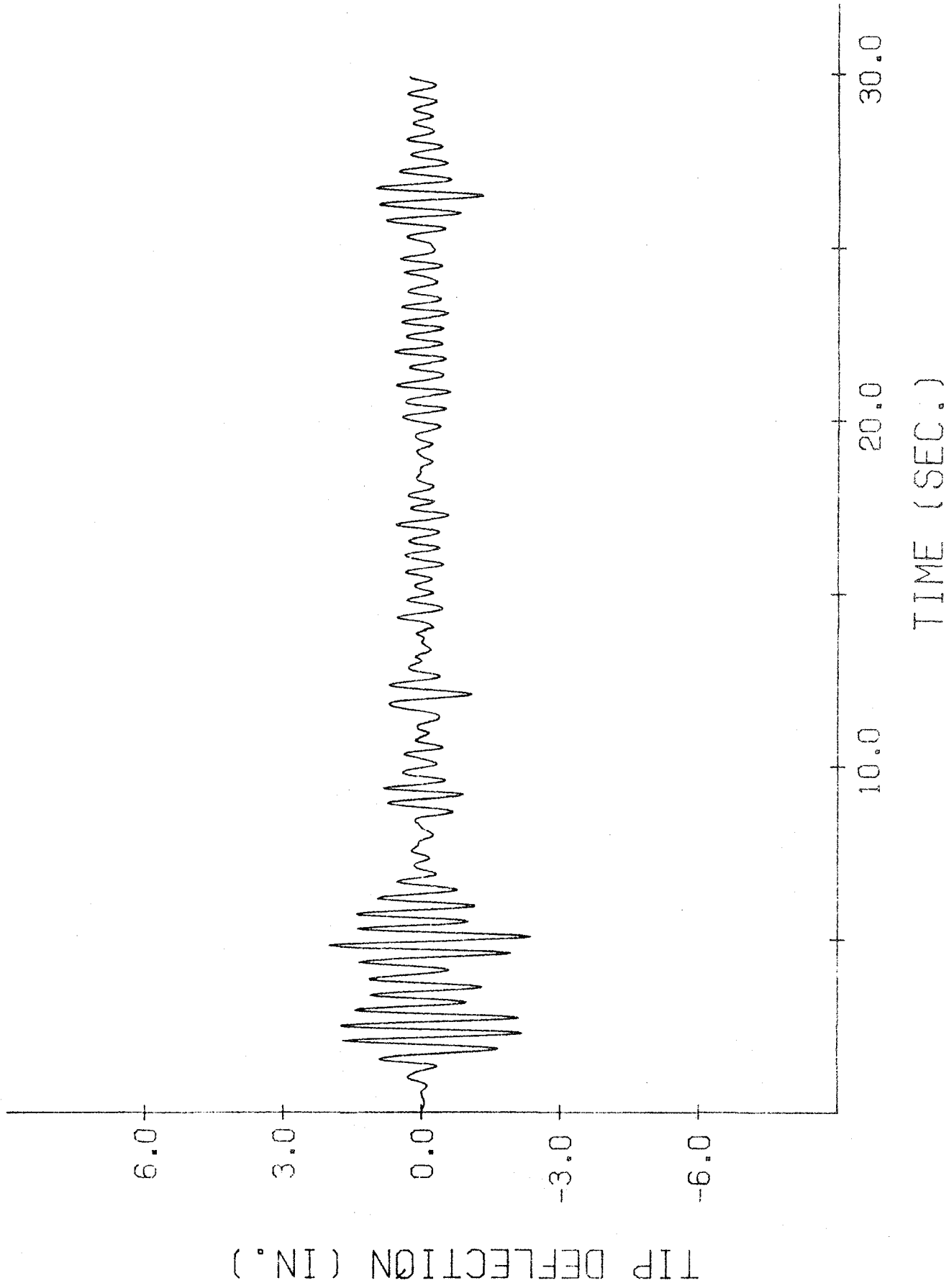


Fig. 29. Tip Deflection at $\theta=0^\circ$ vs. Time Curve for the Paradise Cooling Tower with Damping Coefficient Equal to 7 Percent of its Critical Value.

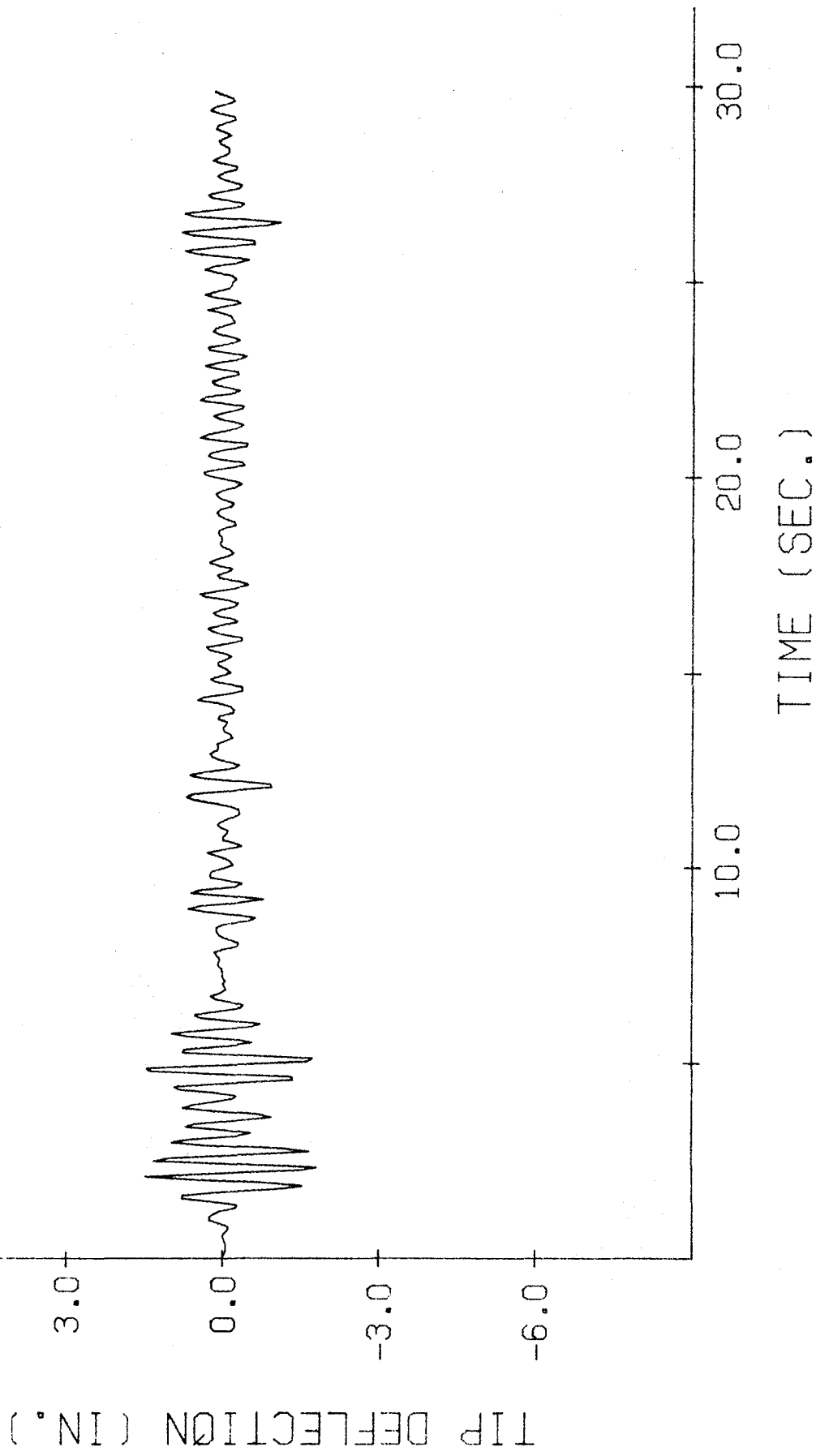


Fig. 30. Tip Deflection at $\theta=0^\circ$ vs. Time Curve for the Paradise Cooling Tower with Damping Coefficient Equal to 10 Percent of its Critical Value.

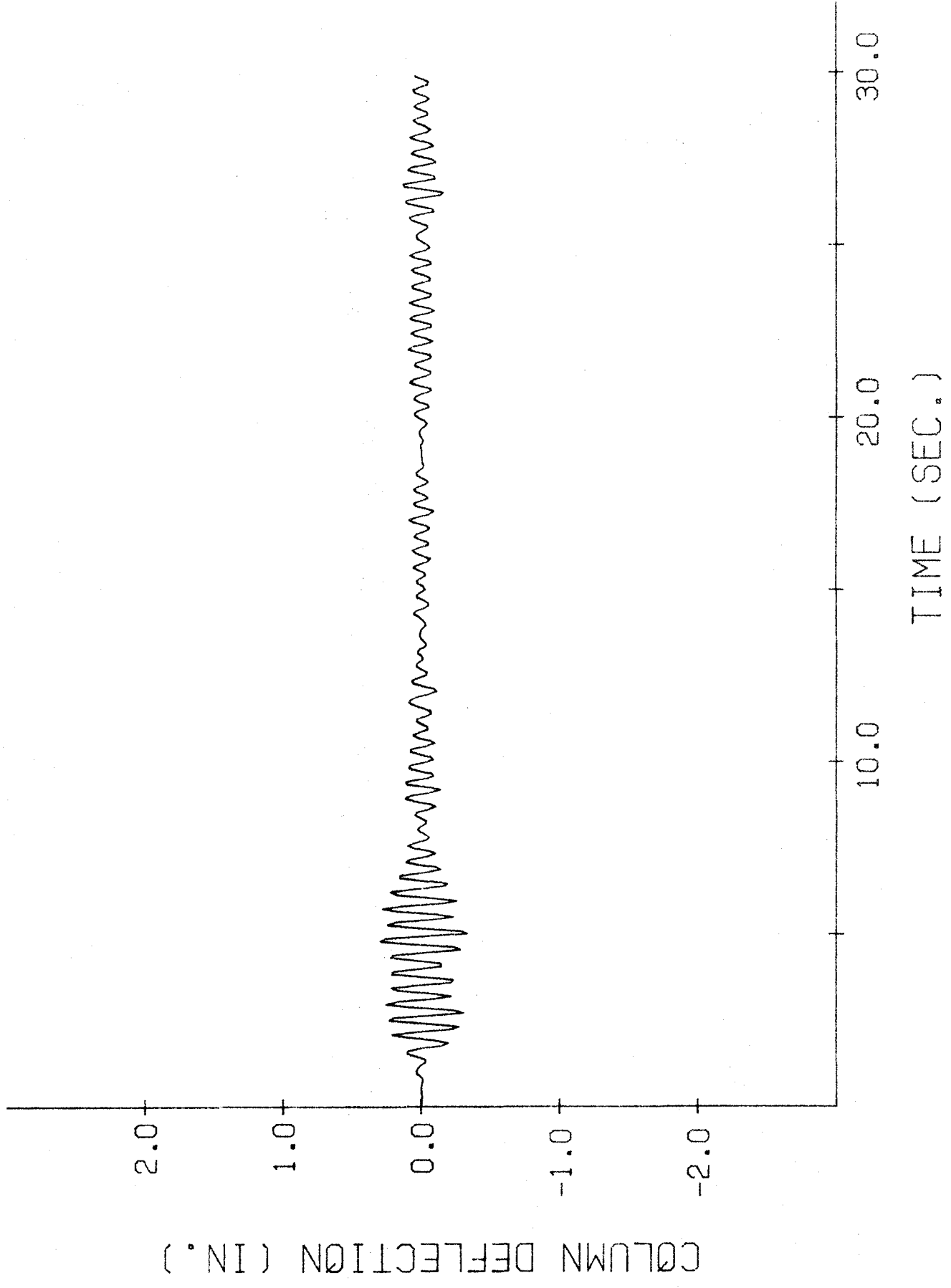


Fig. 31. Deflection at Column Top (at $\theta=0^\circ$) vs. Time Curve for the Paradise Cooling Tower with Damping Coefficient Equal to 4 Percent of its Critical Value.

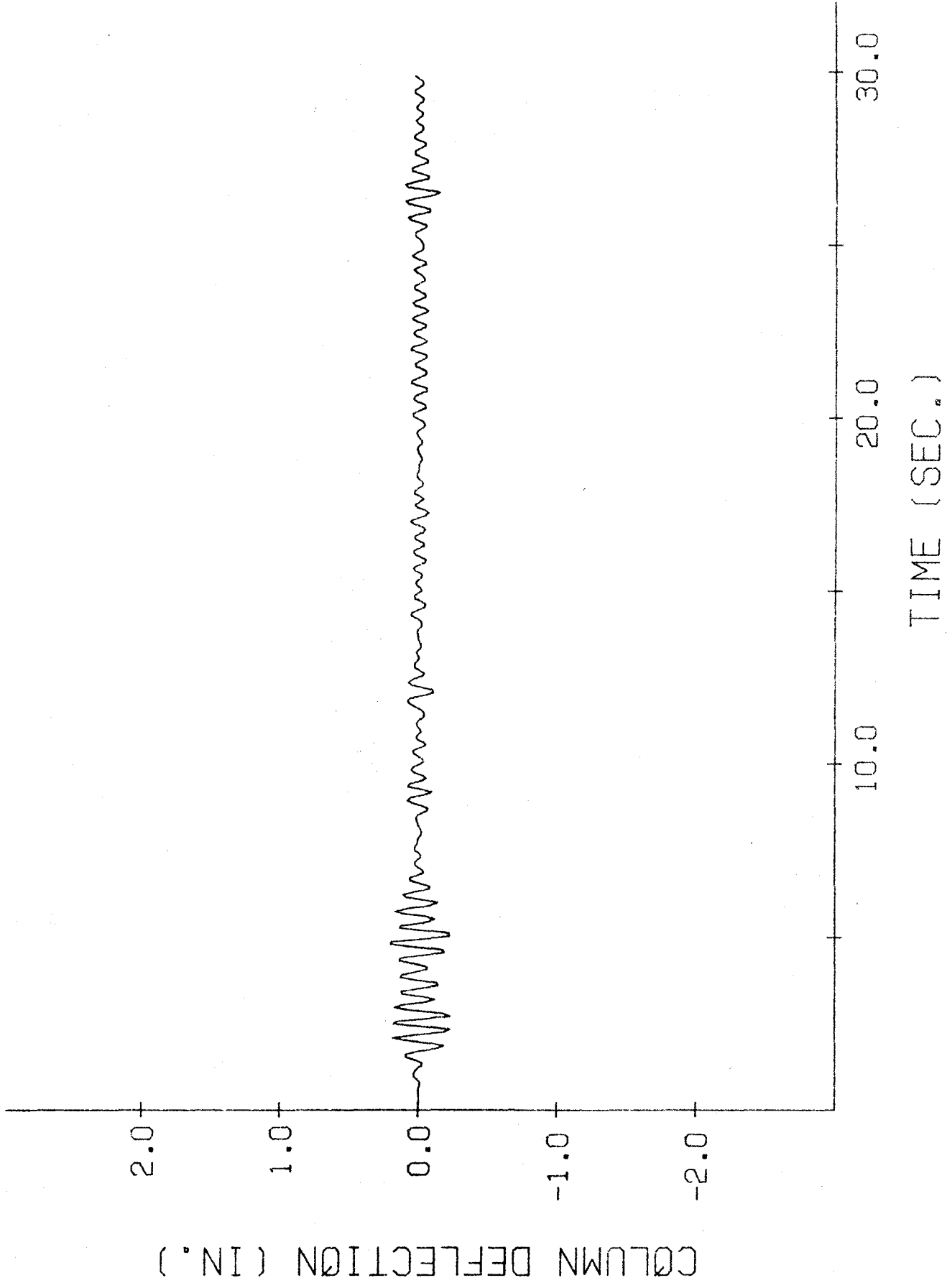


Fig. 32. Deflection at Column Top (at $\theta=0^\circ$) vs. Time Curve for the Paradise Cooling Tower with Damping Coefficient Equal to 7 Percent of its Critical Value.

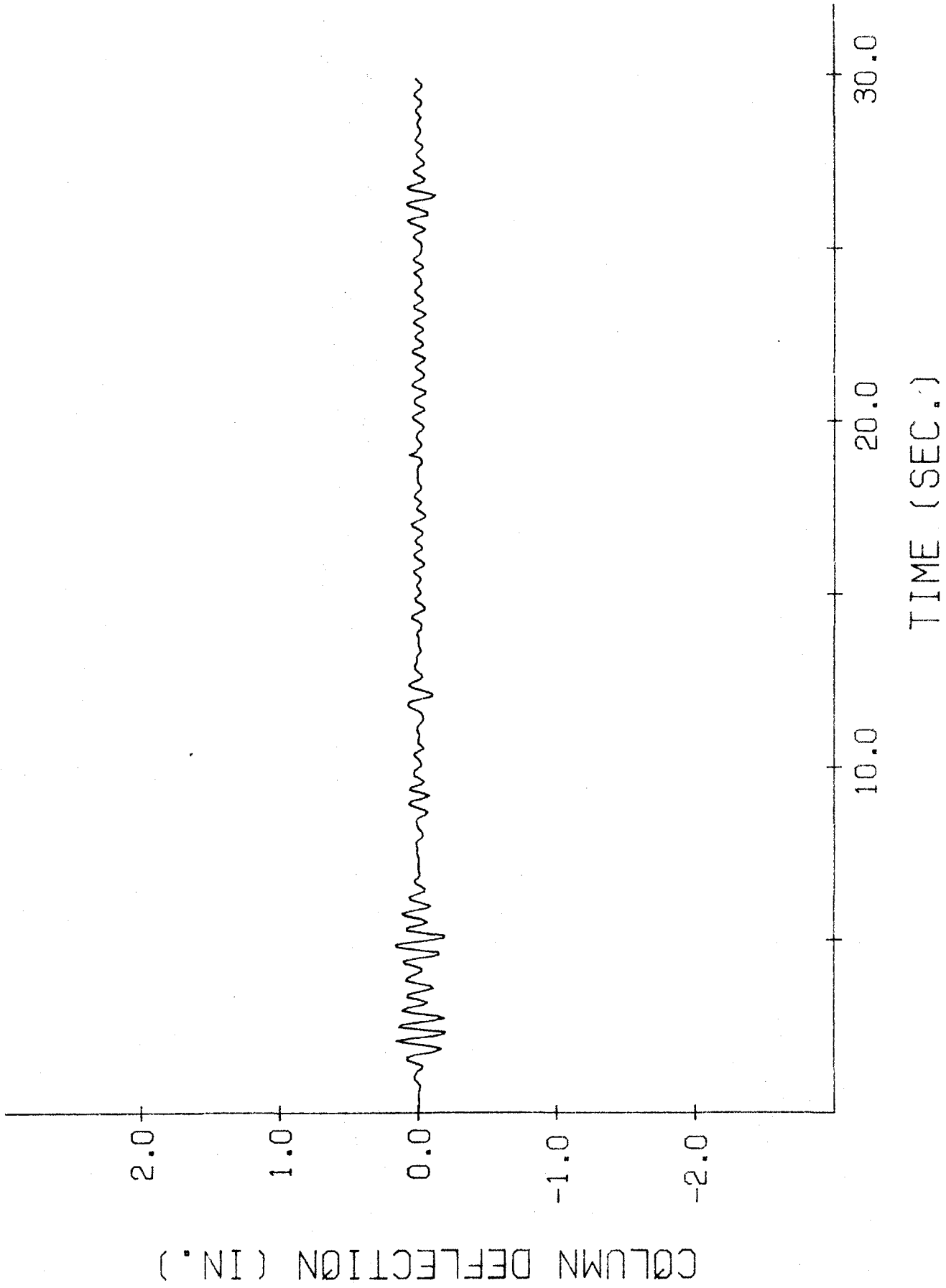


Fig. 33. Deflection at Column Top (at $\theta=0^\circ$) vs. Time Curve for the Paradise Cooling Tower with Damping Coefficient Equal to 10 Percent of its Critical Value.

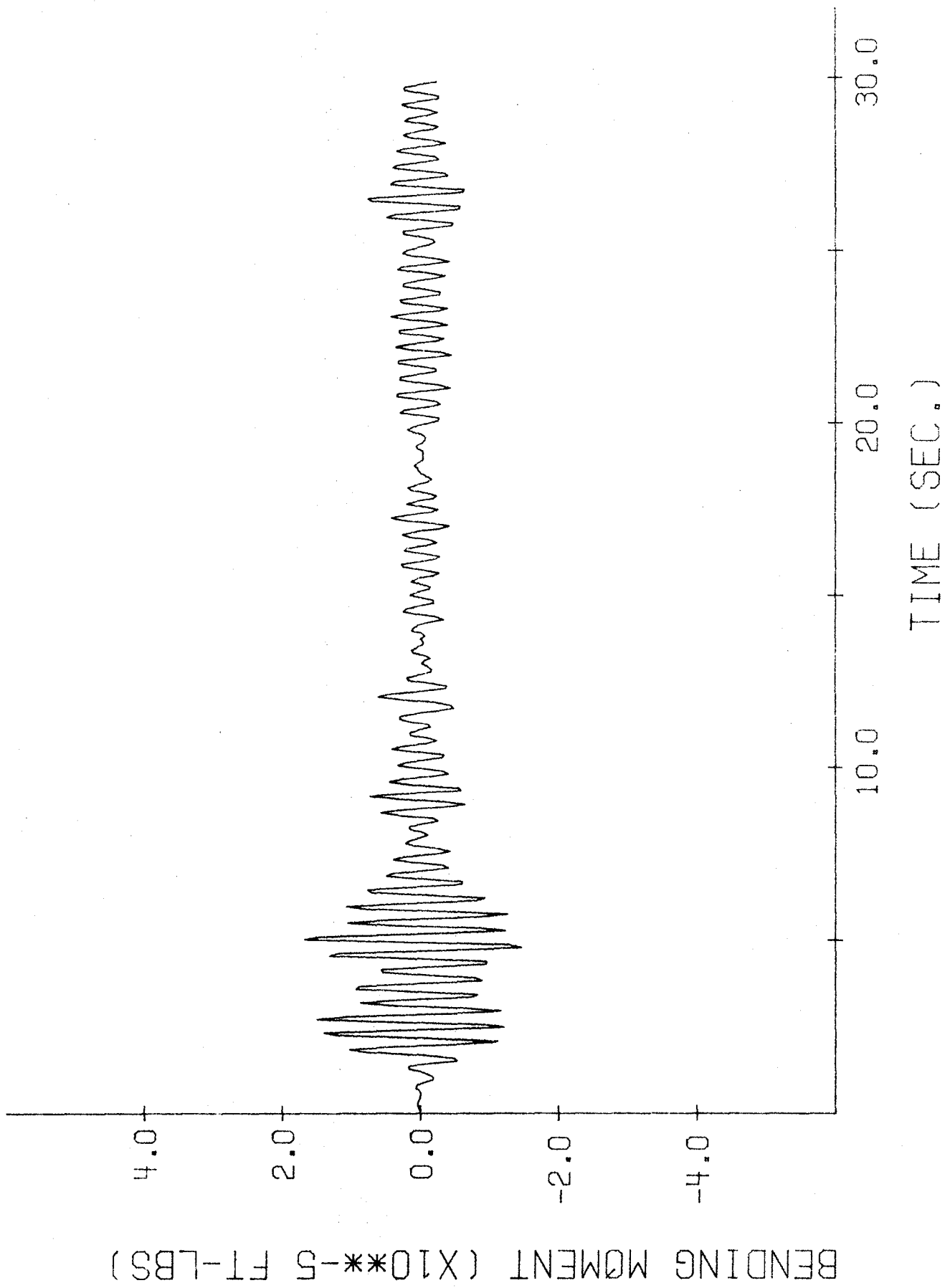


Fig. 34. Bending Moment at Column Top (at $\theta=0^\circ$) vs. Time Curve for the Paradise Cooling Tower with Damping Coefficient Equal to 4 Percent of its Critical Value.

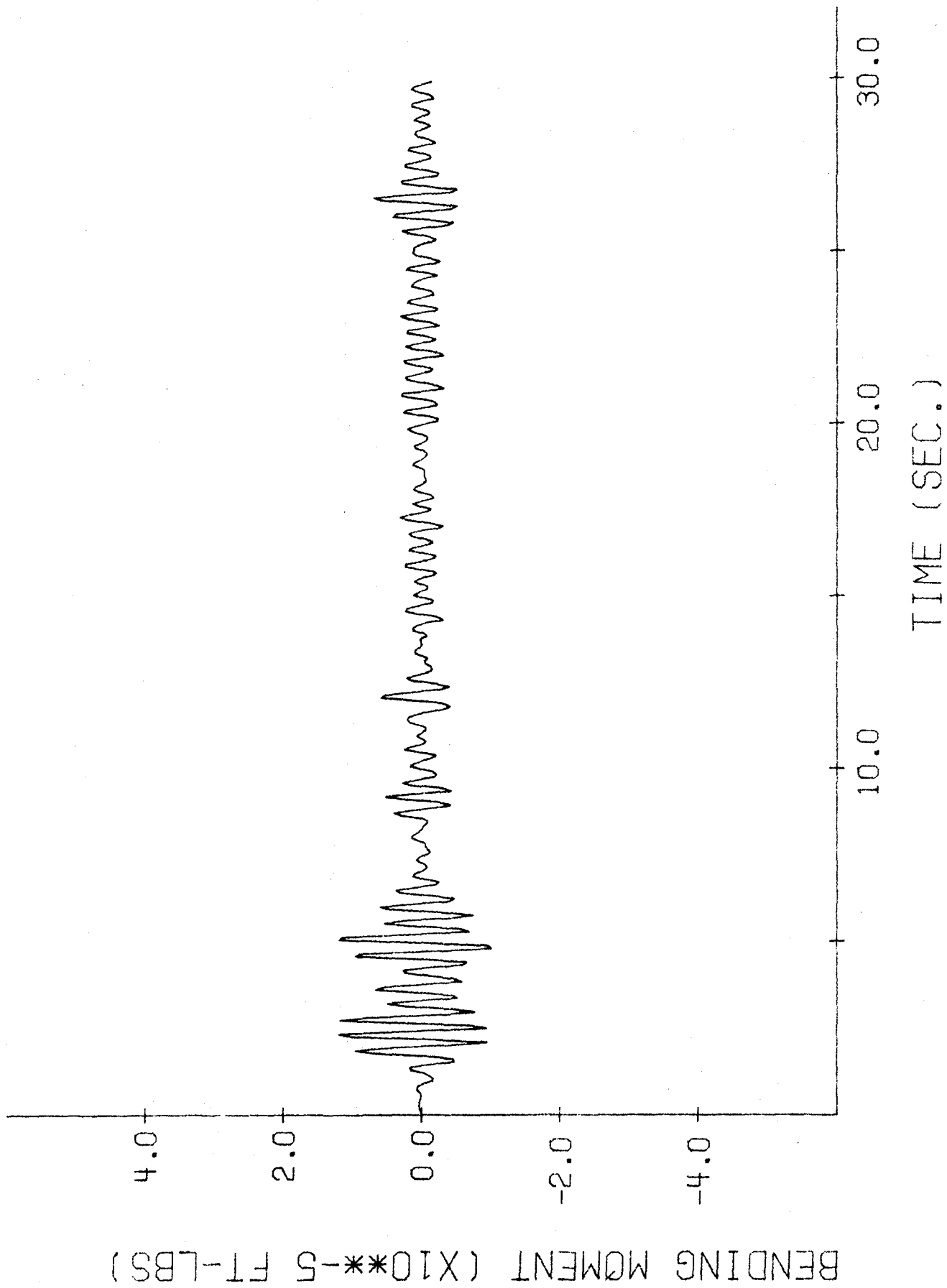


Fig. 35. Bending Moment at Column Top (at $\theta=0^\circ$) vs. Time Curve for the Paradise Cooling Tower with Damping Coefficient Equal to 7 Percent of its Critical Value.

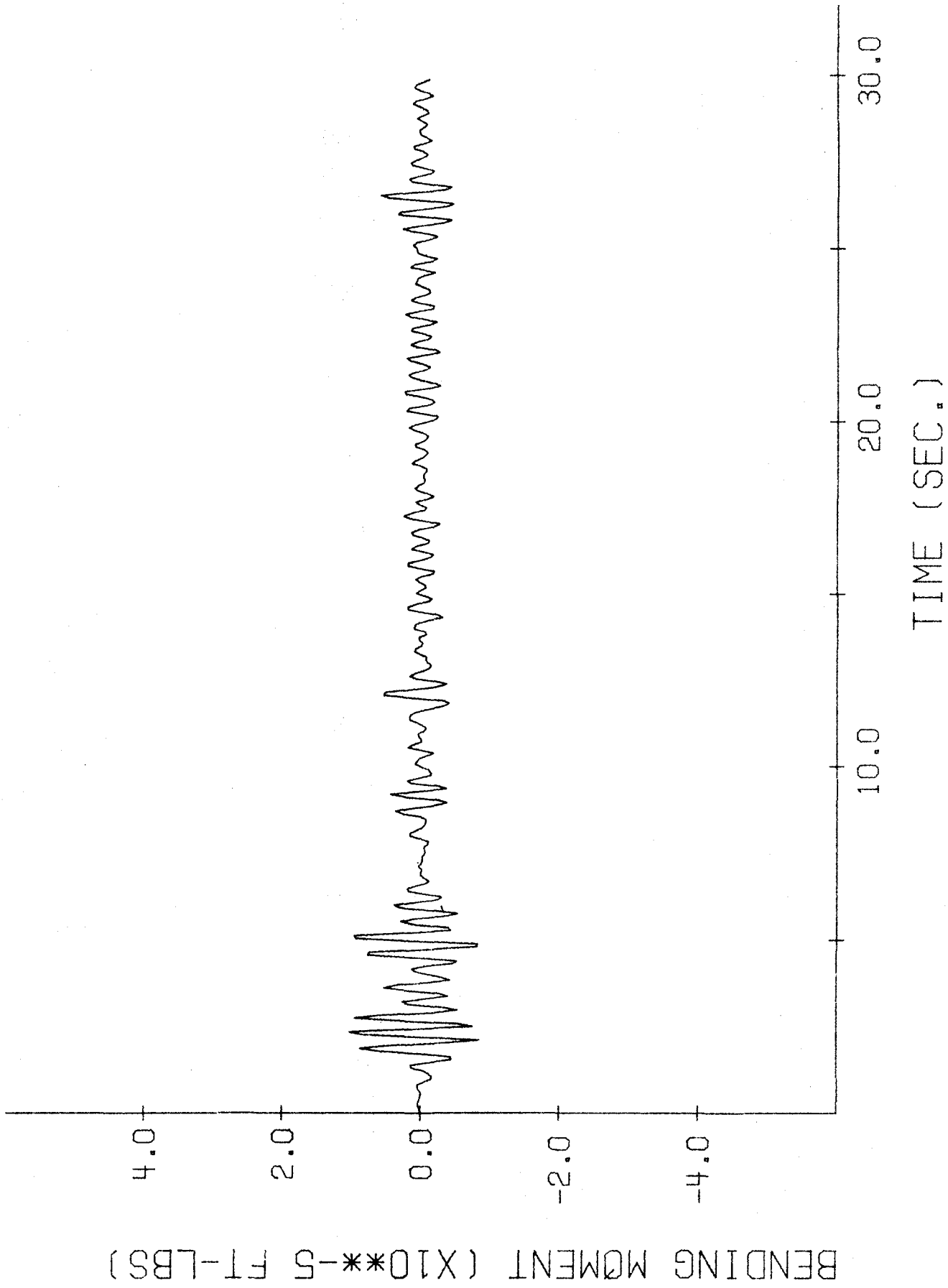


Fig. 36. Bending Moment at Column Top (at $\theta=0^\circ$) vs. Time Curve for the Paradise Cooling Tower with Damping Coefficient Equal to 10 Percent of its Critical Value.

AXIAL FORCE (X10*-6 LBS)

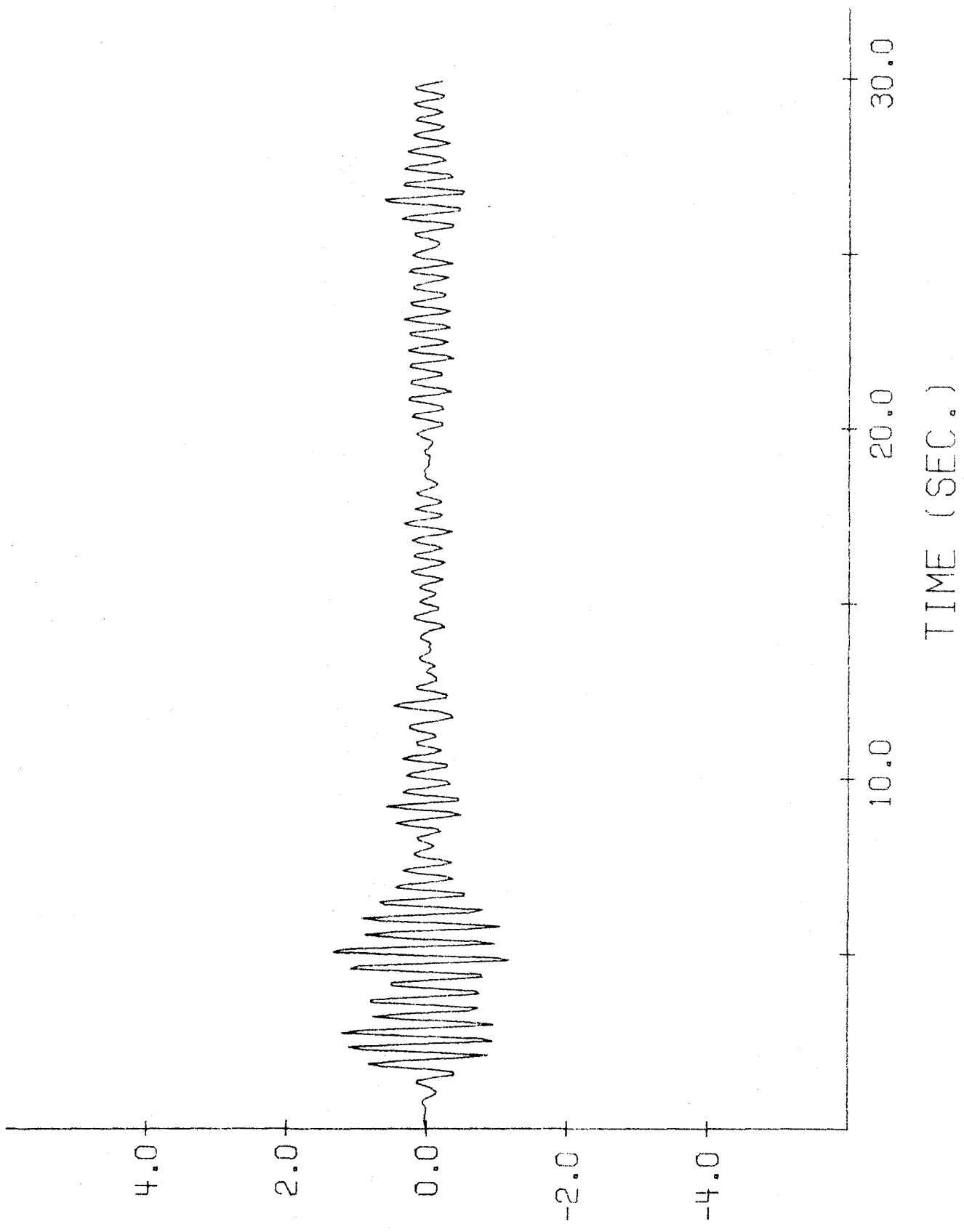


Fig. 37. Axial Force in the Column (at $\theta=0^\circ$) vs. Time Curve for the Paradise Cooling Tower with Damping Coefficient Equal to 4 Percent of its Critical Value.

AXIAL FORCE (X10*-6 LBS)

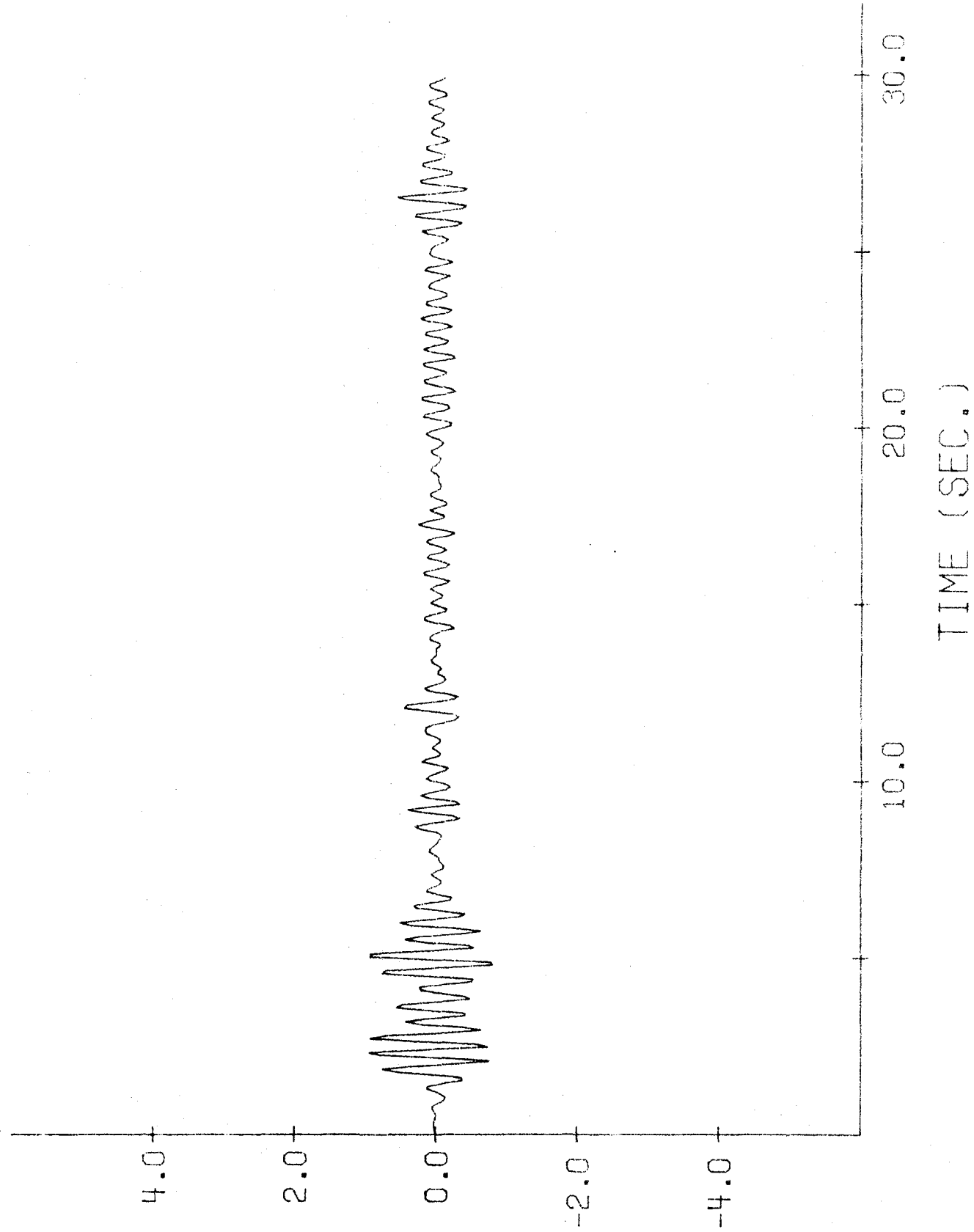


Fig. 38. Axial Force in the Column (at $\theta=0^\circ$) vs. Time Curve for the Paradise Cooling Tower with Damping Coefficient Equal to 7 Percent of its Critical Value.

AXIAL FORCE (X10*-6 LBS)

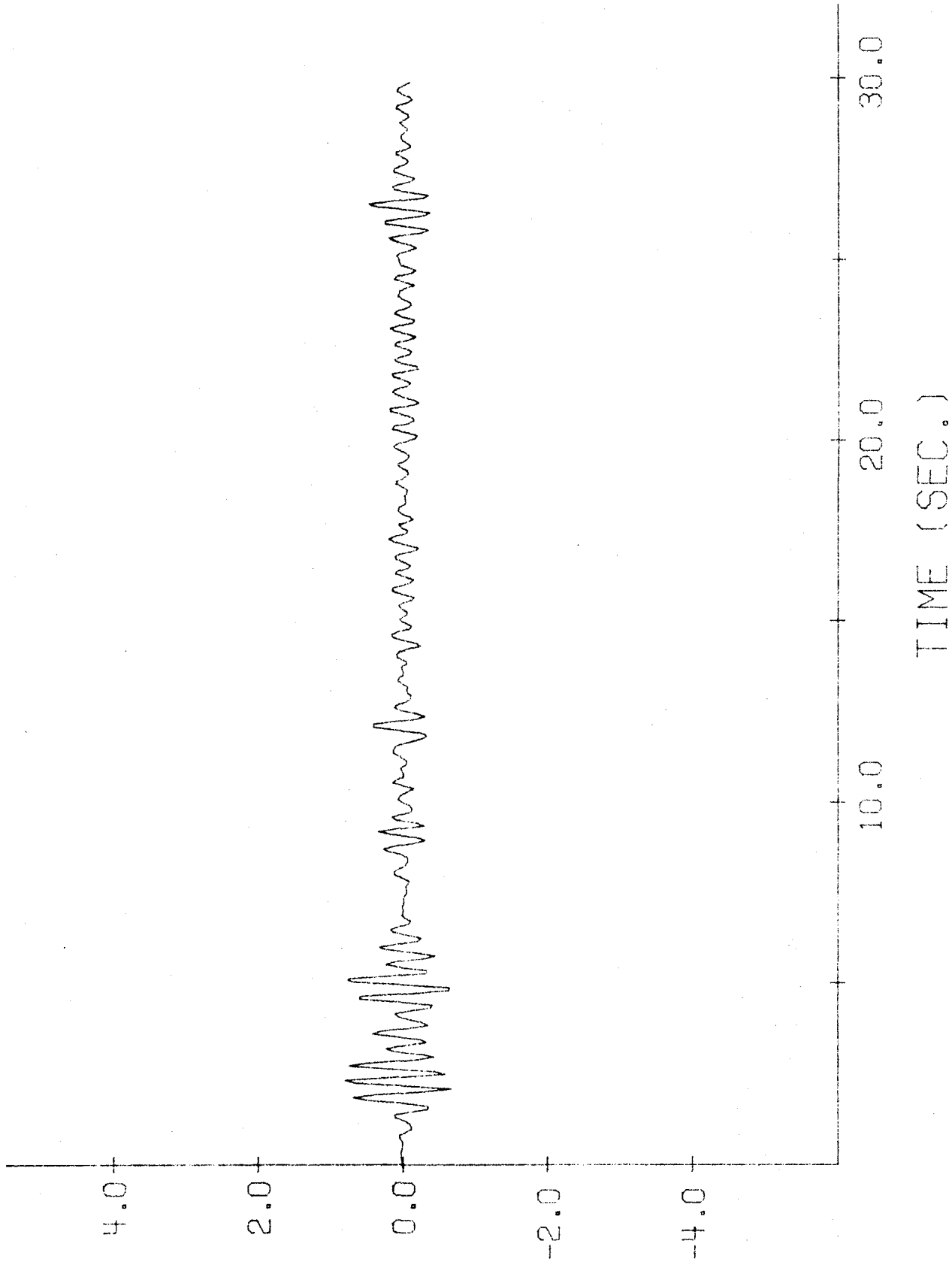


Fig. 39. Axial Force in the Column (at $\theta=0^\circ$) vs. Time Curve for the Paradise Cooling Tower with Damping Coefficient Equal to 10 Percent of its Critical Value.

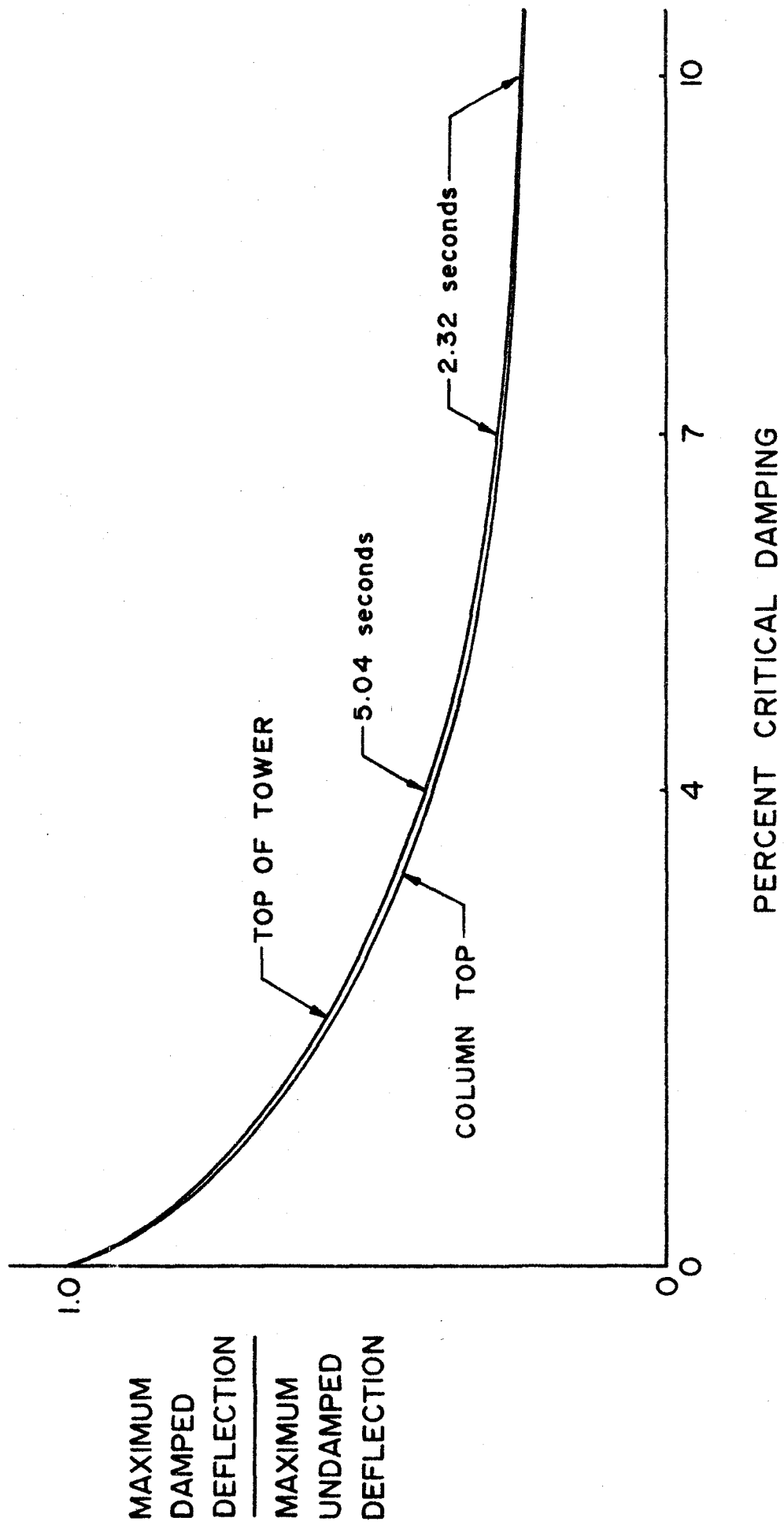


Fig. 40. Variations of Maximum Tip Deflection Ratio and Maximum Column Top Deflection Ratio vs. Damping Coefficient.

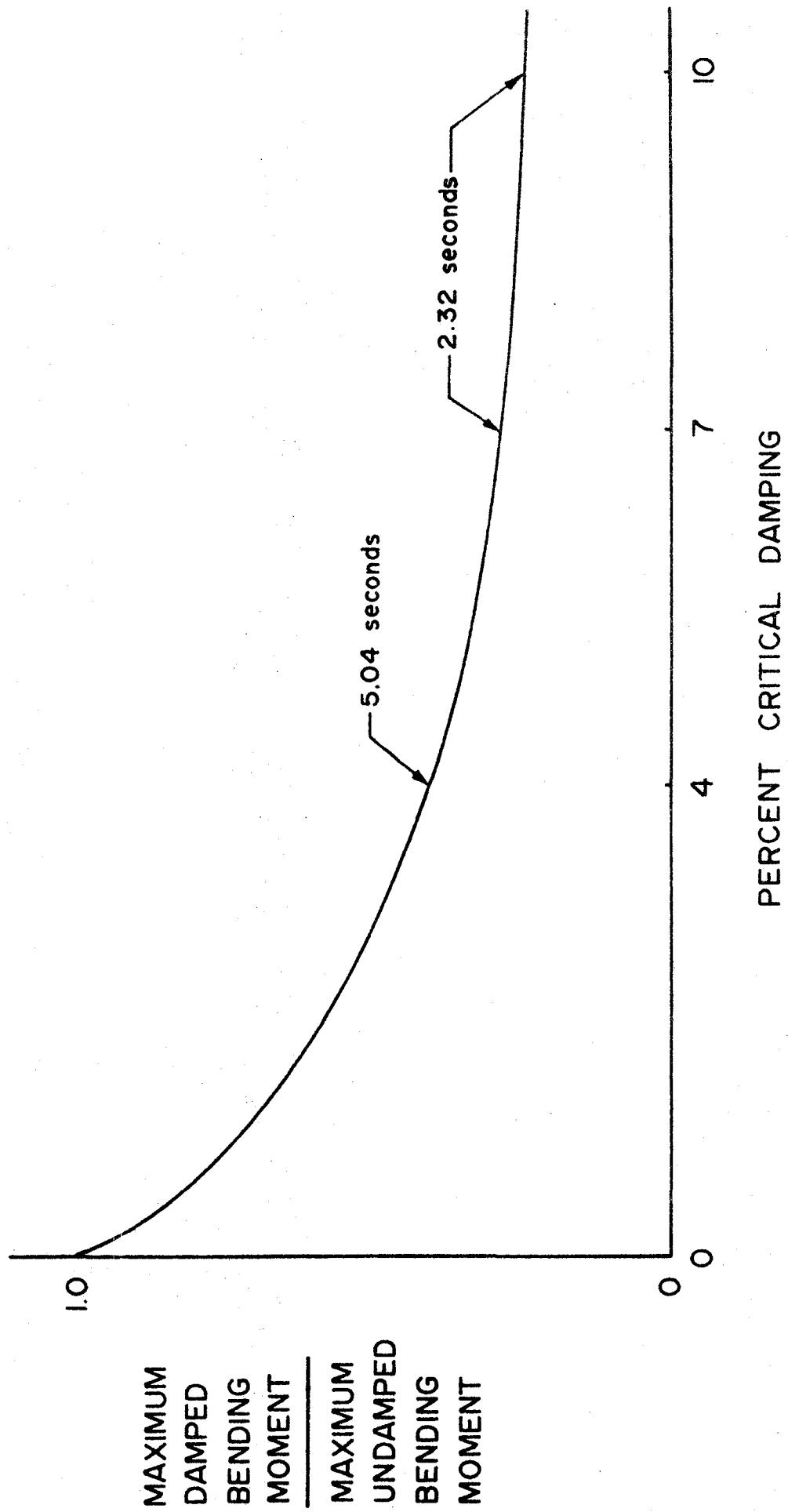


Fig. 41. Variation of Maximum Bending Moment Ratio at Column Top (at $\theta 0^\circ$) vs. Damping Coefficient.

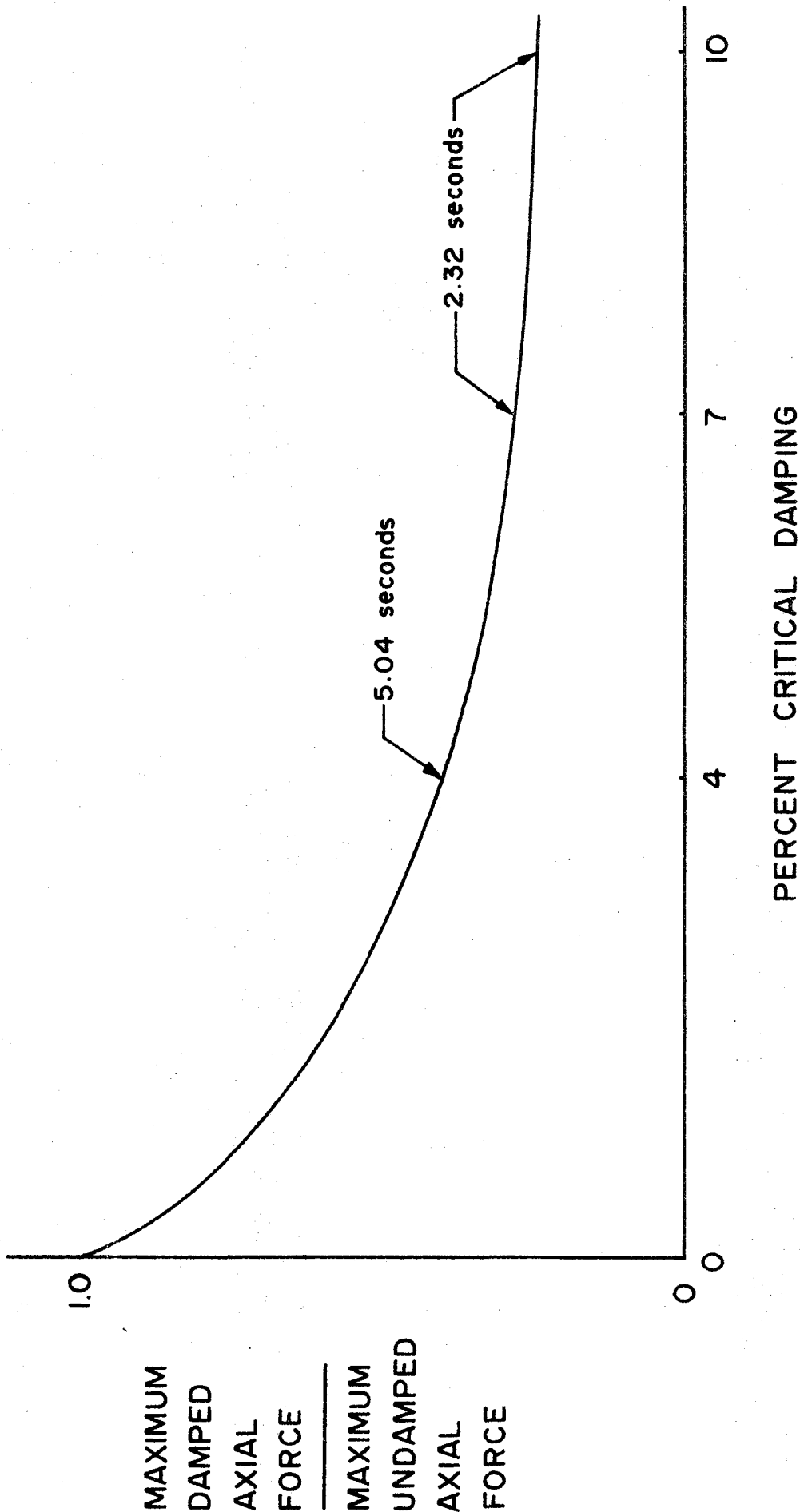


Fig. 42. Variation of Maximum Axial Force Ratio in Column (at $\theta=0^\circ$) vs. Damping Coefficient.